SponGee: A Genetic Tool for Subcellular and Cell-Specific cGMP Manipulation

Oriol Ros, Yvrick Zagar, Solène Ribes, Sarah Baudet, Karine Loulier, Sandrine Couvet, Delphine Ladarre, Alain Aghaie, Alice Louail, Christine Petit, et al.

Resource

Cell Reports

SponGee: A Genetic Tool for Subcellular and Cell-Specific cGMP Manipulation

Graphical Abstract

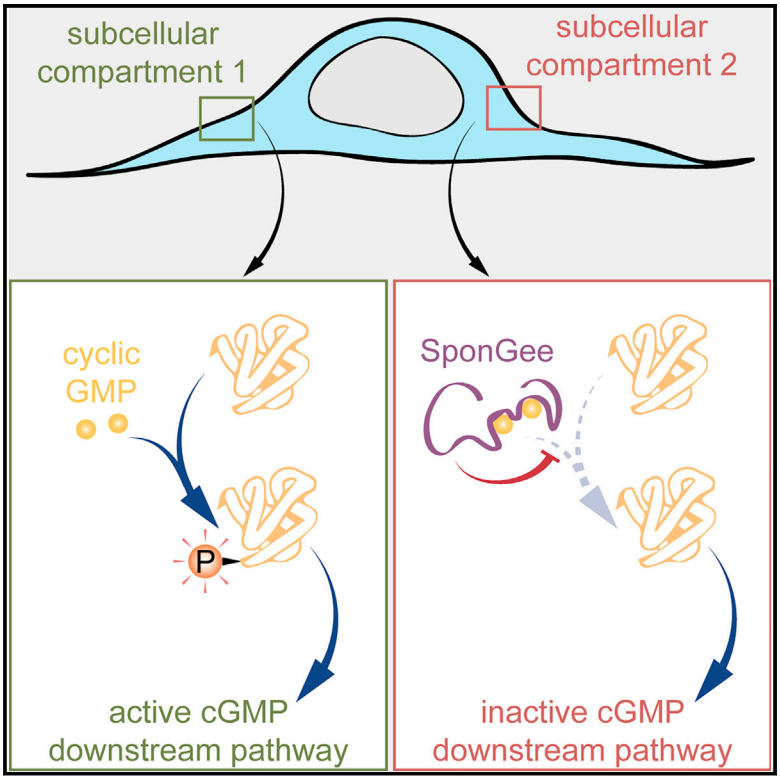

Authors

Oriol Ros, Yvrick Zagar, Solène Ribes, ..., Yves Mechulam, Zsolt Lenkei, Xavier Nicol

Correspondence

xavier.nicol@inserm.fr

In Brief

Ros et al. developed SponGee, a genetically encoded cGMP chelator that enables the manipulation of this second messenger in single cells with subcellular specificity. SponGee alters the migration of developing cortical neurons *in vivo*. Lipid raft targeting of SponGee prevents axon repulsion, in contrast to exclusion from this subcellular compartment.

Highlights

- SponGee is a genetically encoded cGMP scavenger
- SponGee inhibits cGMP-dependent downstream pathways
- SponGee enables cell-specific manipulation of cGMP-dependent processes *in vivo*
- Subcellular targeting confers cell compartment specificity to SponGee

Ros et al., 2019, Cell Reports *27*, 4003–4012
June 25, 2019
https://doi.org/10.1016/j.celrep.2019.05.102

CellPress

Cell Reports
Resource

SponGee: A Genetic Tool for Subcellular and Cell-Specific cGMP Manipulation

Oriol Ros,[1] Yvrick Zagar,[1] Solène Ribes,[1] Sarah Baudet,[1] Karine Loulier,[1] Sandrine Couvet,[1] Delphine Ladarre,[2] Alain Aghaie,[3] Alice Louail,[1] Christine Petit,[3] Yves Mechulam,[4] Zsolt Lenkei,[2,5] and Xavier Nicol[1,6,*]
[1]Sorbonne Université, INSERM, CNRS, Institut de la Vision, 17 rue Moreau, 75012 Paris, France
[2]CNRS, ESPCI-Paris, PSL Research University, Brain Plasticity Unit, UMR 8249, 10 rue Vauquelin, 75005 Paris, France
[3]INSERM, Sorbonne Université, Institut Pasteur, UMR_S 1120, 75012 Paris, France
[4]Laboratoire de Biochimie, Ecole Polytechnique, CNRS UMR 7654, 91128 Palaiseau, France
[5]Université de Paris, Institute of Psychiatry and Neurosciences of Paris, INSERM U1266, 102–108 rue de la Santé, 75014 Paris, France
[6]Lead Contact
*Correspondence: xavier.nicol@inserm.fr
https://doi.org/10.1016/j.celrep.2019.05.102

SUMMARY

cGMP is critical to a variety of cellular processes, but the available tools to interfere with endogenous cGMP lack cellular and subcellular specificity. We introduce SponGee, a genetically encoded chelator of this cyclic nucleotide that enables *in vitro* and *in vivo* manipulations in single cells and in biochemically defined subcellular compartments. SponGee buffers physiological changes in cGMP concentration in various model systems while not affecting cAMP signals. We provide proof-of-concept strategies by using this tool to highlight the role of cGMP signaling *in vivo* and in discrete subcellular domains. SponGee enables the investigation of local cGMP signals *in vivo* and paves the way for therapeutic strategies that prevent downstream signaling activation.

INTRODUCTION

Cyclic guanosine monophosphate (cGMP) is a second messenger involved in a wide range of signaling pathways and cellular processes, including neurotransmission, calcium homeostasis, phototransduction, lipid metabolism, and cation channel activity (Averaimo and Nicol, 2014; Koch and Dell'Orco, 2015; Koesling et al., 2016; Kuhn, 2016). The diversity of these processes suggests that cGMP signals are tightly controlled in space and time to achieve specific modulation of its downstream pathways (Castro et al., 2006; Stangherlin et al., 2011). However, manipulating cGMP is usually achieved using pharmacological approaches that either alter the synthesis or degradation of this cyclic nucleotide or interfere with downstream signaling pathways (Brescia and Zaccolo, 2016; Poppe et al., 2008). These strategies lack both cellular and subcellular specificity. Recently, optogenetic strategies have emerged to impose acute and extrinsic modulation of cGMP or reduce its concentration and to investigate the dynamics of cGMP signaling (Gao et al., 2015; Ryu et al., 2010). However, these light-sensitive tools are handicapped *in vivo*, when light stimulation is technically challenging (e.g., during developmental stages). In addition, photoactivatable guanylyl cyclases do not prevent endogenous cGMP signals ,and the available light-sensitive phosphodiesterases exhibit low specificity for cGMP and degrade the closely related nucleotide cyclic AMP (cAMP) (Gasser et al., 2014; Yoshida et al., 2017). This is a serious drawback because cAMP and cGMP regulate a wide range of signaling pathways and cellular processes that are often modulated by both signaling molecules (e.g., axon pathfinding is dependent on both cAMP and cGMP, which have opposite effects) (Akiyama et al., 2016; Nishiyama et al., 2003; Shelly et al., 2010). These shared regulations make critical the need of tools controlling each cyclic nucleotide with specificity. Genetically encoded tools that monitor or manipulate the concentration of cAMP have fueled the transition from the alteration of this second messenger signals without cellular and subcellular control to the investigation of spatial and temporal codes enabling specificity for its downstream pathways and cellular processes (Averaimo et al., 2016; Lefkimmiatis et al., 2009). The cGMP field is still lacking these essential tools to understand how this ubiquitous second messenger achieves specificity for its myriad of downstream effectors. An attempt has been made with *endless*, an RNA motif that binds cGMP (Kröner et al., 2014). However, *endless* does not enable subcellular control of cGMP manipulation. Expanding this toolbox to peptidic sequences would allow for alteration of physiological variations of cGMP with cellular and subcellular specificity *in vitro* and *in vivo*. The ideal tool with which to manipulate cGMP signaling would (1) prevent the activation of downstream effectors and cGMP-dependent cellular processes; (2) interact directly with cGMP, rather than modifying the activity of cGMP-synthetizing or degrading enzymes; (3) be specific for cGMP over cAMP; (4) be genetically encoded to achieve cellular specificity and enable selective subcellular localization by using fusion to target sequences; and (5) allow cellular identification with fluorescent reporters. We provide here the description of SponGee (sponge-inhibiting cGMP signaling), a cGMP-specific scavenger that fulfills these requirements. Using a FRET sensor we developed, we show that SponGee alters cGMP but not cAMP

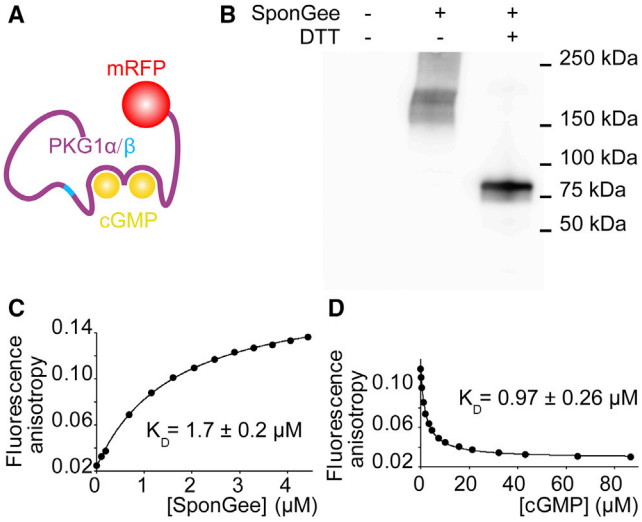

Figure 1. SponGee Dimerizes and Binds cGMP

(A) SponGee contains the cGMP binding domains and leucine zipper of a high-affinity PKG1α/PKG1β chimera (Ruth et al., 1997) and is fused to mRFP to enable cell identification. The effector domains of PKG are deleted in SponGee to avoid the activation of downstream effectors.

(B) SponGee was detected close to its expected monomer molecular weight (67 kDa) under reducing conditions, but at twice this size when DTT was omitted.

(C) The anisotropy of fluorescence emitted by 3.2 nM of Fluo-cGMP exposed to increasing concentration of SponGee was fitted to measure the affinity of SponGee for this cGMP analog.

(D) The fluorescence anisotropy of a mix containing 3.2 nM of Fluo-cGMP, 2 μM of SponGee, and increasing concentrations of cGMP was fitted to determine the dissociation constant of unmodified cGMP.

Number of replicates are provided in Table S1.

signals, has distinct actions depending on its subcellular localization, perturbs axon pathfinding *in vitro*, and disturbs neuronal migration *in vivo*. Because cGMP is a signaling component shared by bacteria (Marden et al., 2011; Ryu et al., 2015) and eukaryotes, this tool will be broadly applicable in a wide range of experimental model systems.

RESULTS

SponGee Buffers Elevations of cGMP

The design of SponGee is based on a high-affinity chimeric variant of the bovine cGMP-dependent protein kinase (PKG) containing fragments of PKG1α and PKG1β (Ruth et al., 1997). SponGee contains the binding sites and chimeric affinity domain of PKG while excluding the kinase domain to prevent the activation of downstream effectors (Figure 1A). The sequence of SponGee is provided in the STAR★Methods section. We further fused the construct to mRFP fluorescent protein for easy identification of SponGee-expressing cells. We favored a PKG-derived scavenger rather than a phosphodiesteterase-based enzyme that would degrade cGMP because of the low specificity of phosphodiesterase-based tools for cGMP over cAMP (Gasser et al., 2014; Yoshida et al., 2017). PKG ability to bind cGMP requires dimerization, a process relying on the leucine zipper of PKG (Kim et al., 2016). This domain is conserved in SponGee. To explore the possibility of SponGee expression as dimers, cellular extracts of HEK293 cells expressing SponGee were analyzed by SDS-PAGE under non-reducing or reducing conditions. In the presence of DTT, SponGee was detected close to its expected monomer size (67 kDa). Under non-reducing conditions, a band corresponding to twice this molecular weight was found, suggesting that SponGee forms dimers (Figure 1B). To characterize its affinity for cGMP, SponGee was expressed in *Escherichia coli* and purified. The dissociation constant was evaluated using fluorescence anisotropy of Fluo-cGMP. The K_D of SponGee for Fluo-cGMP was determined (K_D = 1.7 ± 0.2 μM; Figure 1C), before using a competitive assay to measure the affinity of unmodified cGMP for SponGee (K_D = 0.97 ± 0.26 μM; Figure 1D). Note that because the fluorescence titration data did not exhibit any evidence for two binding sites with different affinities (Figures 1C and 1D), the K_D was computed assuming a single binding site. With the hypothesis of two sites of similar affinities, the K_D of each site would be 1.94 ± 0.52 μM with the following apparent dissociation constant for the entire SponGee protein: K_D = 0.97 ± 0.26 μM.

SponGee buffering properties in living cells were investigated using ^{T}hPDE5^{VV}, a FRET sensor for cGMP that we developed. ^{T}hPDE5^{VV} is similar to cGES-DE5, a previously described cGMP biosensor (Nikolaev et al., 2006). The donor and acceptor fluorescent proteins of cGES-DE5 have been replaced by their optimized variants mTurquoise and a tandem of mVenus, respectively, following a previously described strategy (Klarenbeek et al., 2011). The emission spectrum (434/10 nm excitation) of lysates of HEK293 cells expressing ^{T}hPDE5^{VV} exhibit a shift when in the presence of 200 μM of cGMP, with increased yellow fluorescent protein (YFP) and reduced CFP emission (Figure S1A). The half maximal effective concentration (EC_{50}) of ^{T}hPDE5^{VV} for cGMP was measured from lysates of HEK293 cells expressing the biosensor (EC_{50} = 0.32 ± 0.09 μM; Figure S1B). The same procedure was used to measure the EC_{50} for cAMP (EC_{50} = 1.6 ± 0.7 mM; Figure S1B), highlighting the specificity of this sensor for cGMP over cAMP. ^{T}hPDE5^{VV} was expressed *in vitro* in rat hippocampal neurons exposed to DEA-NONOate, a donor of nitric oxide (NO), which activates cGMP synthesis by SGCs (Bhargava et al., 2013). The elevation of cGMP concentration induced by DEA-NONOate led to a rise of the FRET:CFP ratio in ^{T}hPDE5^{VV}-expressing neurons, validating the use of ^{T}hPDE5^{VV} as a cGMP biosensor (Figures S1C and S1D). In contrast, the adenylyl cyclase activator forskolin did not modify the FRET:CFP ratio, confirming the specificity of ^{T}hPDE5^{VV} for cGMP over the closely related cyclic nucleotide cAMP (Figure S1). HEK293 cells were used to further validate ^{T}hPDE5^{VV} as a cGMP sensor. Although overexpression is generally used to investigate soluble guanylyl cyclase (sGC) activity using this cell line (Mullershausen et al., 2004; Wobst et al., 2016), both α and β subunit of sGC1 are expressed in HEK293 cells (Figure S2A). Spermine-NONOate, a donor of NO that activates sGCs, induces an increase in the phosphorylation of VASP at serine 239, a downstream event of cGMP signaling. ^{p239}VASP elevation is reduced when HEK293 cells are incubated in the sGC inhibitor ODQ (Figure S2B), confirming the presence of sGC activity in HEK293 cells. Like hippocampal neurons,

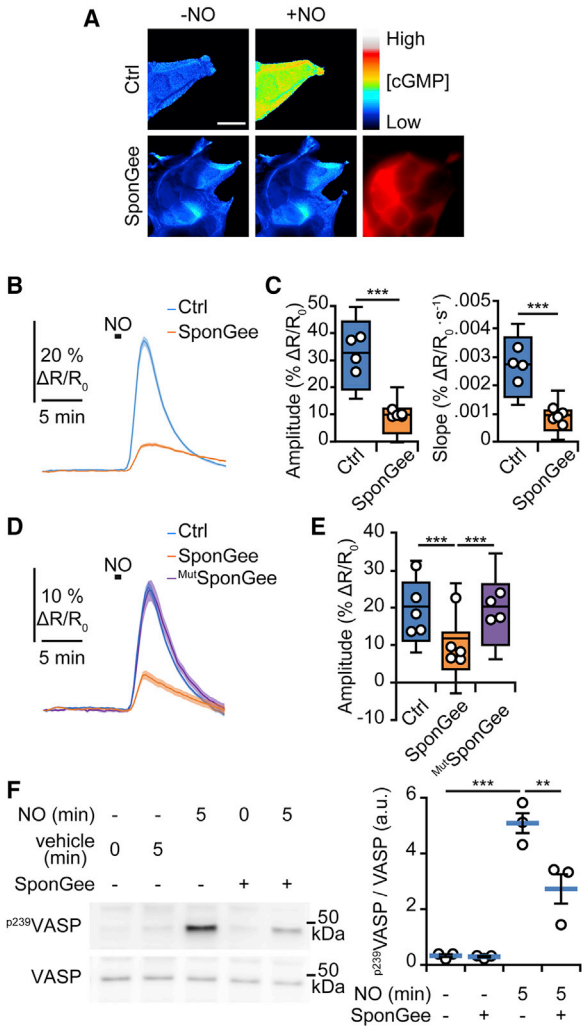

Figure 2. SponGee Is a cGMP Scavenger

(A) A 1-min exposure of 50 μM spermine-NONOate (NO) induces an increase in the cGMP concentration of control HEK293 cells, monitored by the FRET:CFP ratio from the FRET biosensor ^{T}hPDE5^{VV} (B and D, blue trace) (see also Video S1). This elevation is drastically reduced when cells express SponGee (B and D, orange trace) (see also Video S1) but not when a variant of SponGee mutated at both cGMP binding sites is expressed (^{Mut}SponGee, D, purple trace). FRET ratio is coded from blue (low cGMP) to red (high cGMP).

(C and E) The red image (RFP) indicates the expression level of the SponGee-RFP fusion protein. Both the amplitude and rising speed of cGMP elevation are reduced by expression of (C) SponGee but not (E) its mutated form.

(F) NO (50 μM Spermine-NONOate) exposure leads to a ^{p239}VASP increase that is reduced by SponGee expression. Scale bar, 15 μm.

(B and D) Data are mean ± SEM. (C and E) Box-and-whisker plot elements: center line, mean; box limits, upper and lower quartiles; whiskers, SD; mean values for single coverslips (circles) are shown to check for nesting effects. (F) Data are mean ± SEM. Values for individual experiments are shown. (C) ***$p < 0.001$; Mann-Whitney tests. (F) ***$p < 0.001$; **$p < 0.01$; one-way ANOVA and Newman-Keuls post hoc tests. Exact p values and number of replicates are provided in Table S1. CFP and YFP traces together with individual cell examples are provided in Figure S7.

See also Figures S1, S2, and S3.

^{T}hPDE5^{VV}-expressing HEK293 cells exhibited an increase in the FRET:CFP ratio when exposed to a short pulse of spermine-NONOate, revealing an elevation in intracellular cGMP concentration (Figures 2A and 2B; Figure S2; Video S1). The cGMP elevation detected by ^{T}hPDE5^{VV} is reduced by the pharmacological blockade of sGC activity using ODQ (Figures S2C and S2D). These observations demonstrate that the signal detected by ^{T}hPDE5^{VV} relies on sGC activity. To further confirm that ^{T}hPDE5^{VV} is a cGMP sensor, a previously described FRET probe, cGi500, was used (Russwurm et al., 2007). cGi500-expressing HEK293 cells exhibited an elevation in the CFP:FRET ratio of reduced amplitude compared to ^{T}hPDE5^{VV} after a 1-min pulse of NO exposure (Figures S2E and S2F). The reversibility of the FRET change of ^{T}hPDE5^{VV} was complete, in contrast to cGi500 that did not reach its basal CFP:FRET ratio after the wash of NO (Figures S2E and S2G).

In the absence of SponGee, a 1-min pulse of spermine-NONOate induced an increase in the FRET:CFP ratio of ^{T}hPDE5^{VV} with a 1-min delay since the start of the stimulation (Figures 2A–2C; Video S1). SponGee expression resulted in a profound reduction of the spermine-NONOate-induced FRET:CFP change, reflecting a decrease in cGMP molecules available to bind the biosensor (Figures 2A–2C; Video S1). To verify that the activity of SponGee is linked to its cGMP binding sites, both binding domains were mutated following a previously used strategy to prevent cAMP binding to the cyclic nucleotide binding domain of PKA (Lefkimmiatis et al., 2009): the glycine residues at positions 247 and 299 were converted into glutamic acid. These two point-mutations were sufficient to abolish the reduction in the FRET response induced by SponGee (Figures 2D and 2E), excluding the possibility that SponGee is a NO scavenger through cysteine nitrosylation or the formation of disulfide bonds in SponGee. It also excludes the possibility that the detected FRET variation is due to disulfide bonds in other proteins, including the FRET sensor. To evaluate whether the SponGee-induced reduction in the FRET amplitude is transferable to other cGMP FRET sensors, we reproduced similar experiments with cGi500. Like ^{T}hPDE5^{VV}, cGi500 enabled the detection of a NO-induced cGMP elevation in HEK293 cells, which was reduced when SponGee was co-expressed (Figures S3A and S3B). SponGee expression is also sufficient to reduce NO-induced VASP phosphorylation (Figure 2F). These observations demonstrate that SponGee works as a cGMP scavenger and reduces the availability of this second messenger for its downstream pathway activation. It also highlights that SponGee is more effective in scavenging cGMP than the binding domains of both ^{T}hPDE5^{VV} and cGi500 because it competes with these biosensors to bind the available cGMP and that the cGMP-induced changes in the FRET ratio is reduced by SponGee expression. Because cGMP scavenging relies on the availability of the cGMP binding sites, the intracellular concentration of SponGee might strongly affect its efficiency to reduce endogenous cGMP signals due to the saturation of the binding pockets. To evaluate the impact of the expression level, single-cell SponGee concentration was estimated using the fluorescence intensity of the fused mRFP and plotted against the amplitude of the FRET ratio for individual cells. Although a few cells with the lowest expression of SponGee exhibited low or no cGMP

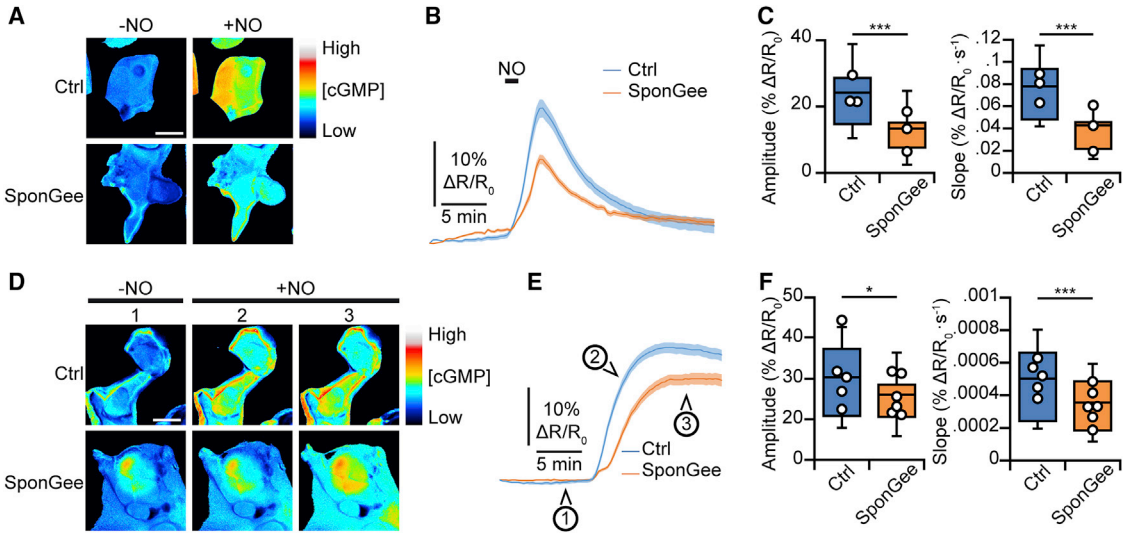

Figure 3. SponGee Reduces the Elevation of cGMP Concentration Induced by a Prolonged Pulse of Spermine-NONOate and Delays Massive and Sustained Elevations of Intracellular cGMP Concentration

(A) HEK293 cells were exposed to a 2-min pulse of 50 μM spermine-NONOate.

(B and C) SponGee-expressing cells (B, orange trace) display (C) a reduction of both the FRET:CFP ratio amplitude and the rate of increase compared to controls (also see Video S2).

(D) A 15-min pulse of 50 μM spermine-NONOate induces a massive change in the ^{T}hPDE5^{VV} FRET:CFP ratio.

(E and F) Cells expressing SponGee (E, orange trace) exhibit a change in the FRET:CFP ratio (F) of similar magnitude, but delayed as compared to cells devoid of SponGee (E, blue trace; also see Video S3). Scale bar, 20 μm.

(B and E) Data are mean ± SEM. (C and F) Box-and-whisker plot elements: center line, mean; box limits, upper and lower quartiles; whiskers, SD; mean values for single coverslips (circles) are shown to check for nesting effects. *$p < 0.05$, ***$p < 0.001$; Mann-Whitney test. Exact p values and number of replicates are provided in Table S1. CFP and YFP traces together with individual cell examples are provided in Figure S7.

buffering, the reduction the ratio elevation was observed in most cells, including those with low mRFP fluorescence (Figure S3C).

To investigate the limits of cGMP buffering by SponGee, cells co-expressing SponGee and ^{T}hPDE5^{VV} were exposed to longer spermine-NONOate stimulation (2-min pulse or sustained exposure). Expressing SponGee was sufficient to reduce both the amplitude and delay of the FRET:CFP elevation induced by a 2-min exposure to spermine-NONOate (Figures 3A–3C; Video S2). In contrast, the cGMP elevation detected by ^{T}hPDE5^{VV} during a sustained spermine-NONOate stimulation was delayed, but the peak amplitude was only moderately reduced (Figures 3D–3F; Video S3). This suggests that massive and prolonged increase in cGMP concentration leads to the saturation of SponGee or ^{T}hPDE5^{VV} cGMP binding sites.

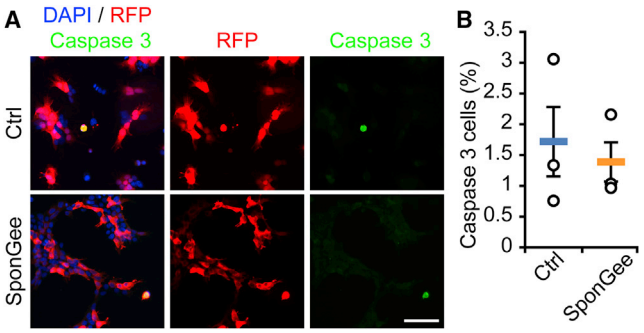

Figure 4. SponGee Does Not Affect Cell Survival

(A) HEK293 cells were transfected with either SponGee or RFP. Activated Caspase 3-positive cells were immunolabeled to evaluate the number of cells undergoing apoptosis.

(B) SponGee-expressing cells are not more prone to enter an apoptotic program than their RFP-expressing controls.

(A) Scale bar, 50 μm. (B) Data are mean ± SEM with individual data points, Mann-Whitney test. Exact p values and number of replicates are provided in Table S1.

SponGee Is Not Cytotoxic

The chronic scavenging of cGMP might affect cell survival because of the role of this second messenger in many signaling pathways and cellular processes. However, the morphology of SponGee-expressing cells did not differ from their control, suggesting that cell death was not affected (Figure 4A). Activated Caspase 3 was immunostained to evaluate the fraction of apoptotic cells. Caspase 3 was not activated in SponGee-expressing HEK293 cells, confirming that buffering cGMP with SponGee does not affect cell survival (Figure 4).

SponGee Is Specific for cGMP Over cAMP

To evaluate the specificity of SponGee for cGMP over the closely related cAMP, we conducted FRET experiments by using a previously described and validated cAMP biosensor,

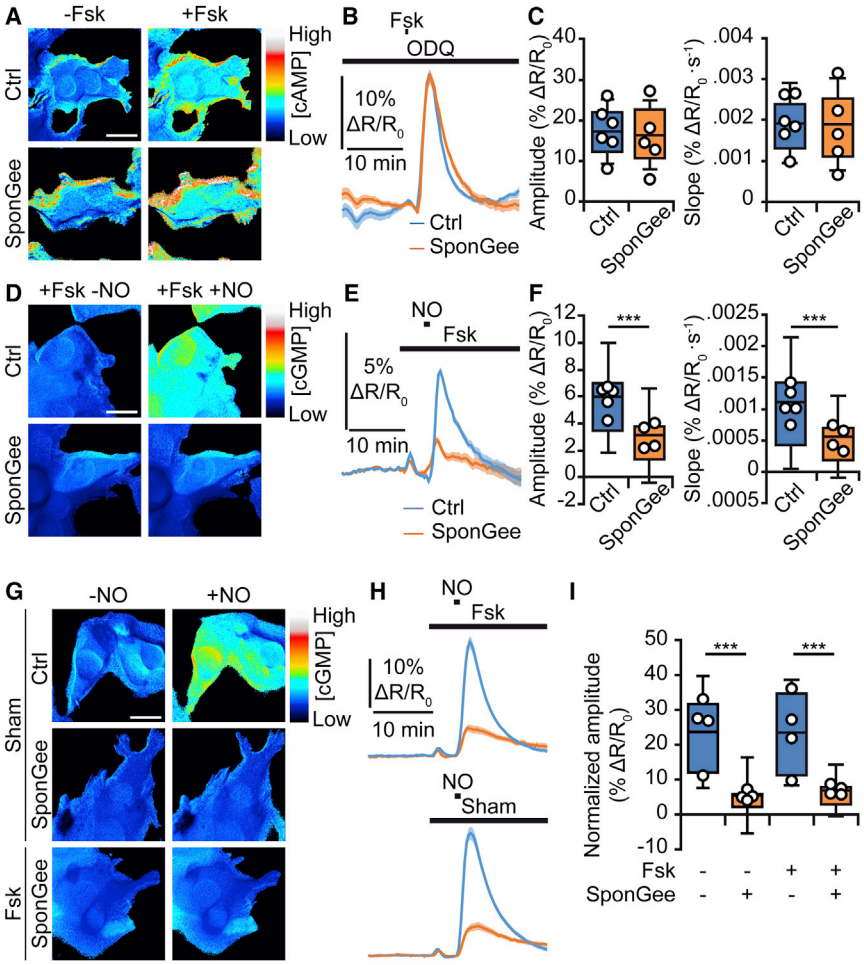

Figure 5. SponGee Is Highly Specific for cGMP Over cAMP

(A) HEK293 cells were exposed to a 20-s pulse of 10 μM Fsk under constant 10 μM ODQ perfusion.

(B and C) The SponGee-positive cells (B, orange trace) co-expressing the cAMP biosensor H147 display (C) a similar CFP:FRET ratio amplitude and rate of increase compared to controls (B, blue trace; also see Video S4).

(D) Cells were exposed to 10 μM Fsk to elevate their cAMP concentration and challenge the ability of SponGee to discriminate between cGMP and cAMP. Fsk-elevated cAMP concentration did not prevent SponGee (E, orange trace) to reduce (F) the amplitude and rate of increase of the 50 μM Spermine-NONOate-induced cGMP signal detected by the cGMP sensor ^{T}hPDE5^{VV} (also see Video S5).

(G) A second set of experiments was carried out to compare the reduction of cGMP elevation in presence or absence of 10 μM Fsk.

(H and I) Fsk exposure (H, top) does not reduce (I) the ability of SponGee to buffer cGMP elevation. Scale bar, 20 μm.

(B, E, and H) Data are mean ± SEM. (C, F, and I) Box-and-whisker plot elements: center line, mean; box limits, upper and lower quartiles; whiskers, SD; mean values for single coverslips (circles) are shown to check for nesting effects. ***$p < 0.001$; Mann-Whitney test. Exact p values and number of replicates are provided in Table S1. CFP and YFP traces together with individual cell examples are provided in Figure S7.

H147 (Averaimo et al., 2016; Klarenbeek et al., 2015). In many systems, cAMP and cGMP signaling influence each other, with the concentration of both cyclic nucleotides changing in opposite directions (Averaimo and Nicol, 2014; Pietrobon et al., 2011; Shelly et al., 2010; Zaccolo and Movsesian, 2007). To minimize the influence of cGMP scavenging by SponGee on cAMP measurements, the cAMP buffering activity of SponGee was evaluated in cells with pharmacologically reduced and stabilized cGMP concentration. RFP- or SponGee-expressing cells were maintained with reduced cGMP-signaling by using the sGC inhibitor ODQ and later exposed to a 20-s pulse of the adenylyl cyclase activator Forskolin (Fsk). SponGee did not reduce the amplitude or induce a delay in the elevation of cAMP concentration (Figures 5A–5C; Video S4). We evaluated whether high intracellular concentrations of cAMP can bind and saturate the cGMP-binding domains of SponGee, reducing its ability to act as a cGMP-specific scavenger. SponGee is still able to efficiently buffer NO-induced cGMP elevation while cAMP concentration is increased by Fsk (Figures 5D–5F; Video S5). An additional set of experiments was carried out to evaluate whether the reduction in the FRET:CFP ratio is similar with and without cAMP elevation. Fsk exposure does not affect the SponGee-induced reduction in the cGMP signal, showing that cellular cAMP does not prevent SponGee to buffer cGMP, even in a cellular environment with high cAMP concentrations (Figures 5G–5I). These observations demonstrate that SponGee does not buffer intracellular cAMP and highlight its specificity for cGMP.

SponGee Reveals the Requirement of cGMP for Neuronal Migration *In Vivo*

To evaluate the ability of SponGee to interfere with physiological processes *in vivo* and, thus, assess its potential as a tool to investigate cellular function in an intact organism, SponGee was electroporated *in utero* in the brain lateral ventricles of embryonic day 14.5 (E14.5) mouse embryos. The migration of electroporated cortical neurons was analyzed at E18.5 and P10. In E18.5 control eGFP and mRFP co-electroporated animals, neurons display an archetypical migration with the majority of transfected cells accumulating in the cortical plate near the marginal zone (Figures 6A and 6B). In contrast, neurons co-electroporated with SponGee and GFP exhibit a delayed migration, with neurons scattered throughout the cortical plate, including the intermediate zone (Figure 6A). In addition, several electroporated cells failed to stall at the cortical plate, overshooting the terminal zone observed in mRFP-electroporated controls (Figure 6B). Heterotopias

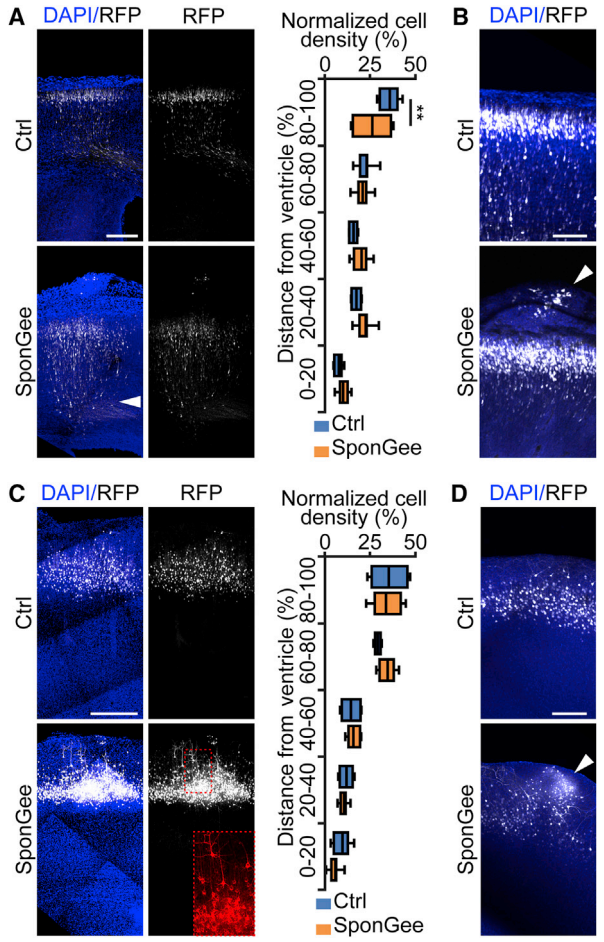

Figure 6. SponGee Alters Cortical Neuron Migration *In Vivo*

(A and B) Control cortical neurons electroporated at E14.5 are packed into a dense layer close to the marginal zone at E18.5. In contrast, SponGee expression prevents the development of this layer, with (A) neurons scattered throughout the depth of the developing cortex (arrowhead) and (B) the formation of heterotopias (arrowhead) at the surface of the cortex.

(C) At P10, SponGee-electroporated neurons and their mRFP-electroporated controls are both found in the superficial layers of the cortex. The inset shows mRFP fluorescence, highlighting that SponGee is still expressed at P10.

(D) Heterotopias induced by SponGee at embryonic stages are maintained in P10 pups (arrowhead), indicating that altering cGMP signaling interferes with cortical neuron migration. Box-and-whisker plot elements: center line, mean; box limits, upper and lower quartiles; whiskers, SD.

Scale bars, (A) 250 μm, (B) 100 μm, (C) 500 μm, (D) 200 μm. **$p < 0.01$; Two-way ANOVA and Bonferroni post hoc tests. Exact p values and number of replicates are provided in Table S1.

were found in 7 out of 9 SponGee-electroporated animals, whereas 2 out of 10 mRFP-expressing embryos exhibited neurons overshooting the cortical plate ($p = 0.000037$, χ^2 test). Misplaced SponGee-expressing neurons were still found at P10 with heterotopias in 71% of the pups (5 out of 7) as compared to 20% control animals (1 out of 5, $p = 0.000024$, χ^2 test) (Figures 6C and 6D). This demonstrates that cGMP buffering by SponGee is sufficient to alter the physiological cGMP modulation required for the appropriate neuronal migration *in vivo*.

Subcellular Targeting of SponGee Reveals Local cGMP Signaling during Axon Pathfinding

To achieve specific activation of its plethoric downstream targets, cGMP signals are confined to specific subcellular compartments (Castro et al., 2006; Stangherlin et al., 2011). Because genetic encoding confers the ability to restrict the expression of the constructs to a specific organelle using targeting sequences, we assessed the functionality of SponGee in this scenario. The cGMP buffer was targeted to the plasma membrane, further restricting its expression to the lipid raft microdomains by the N-terminal fusion of a tandem of palmitoylation-myristoylation targeting peptides from Lyn Kinase (Lyn-SponGee) or excluding it from the lipid raft domain by the C-terminal fusion of a CaaX-polylysine motif derived from K-Ras (SponGee-Kras) (Figure 7A) (Averaimo et al., 2016; Depry et al., 2011; Zacharias et al., 2002). We confirmed that Lyn-SponGee and SponGee-Kras expression was restricted to the membrane in HEK293 cells, in contrast to the untargeted SponGee (Figure 7B). We analyzed the localization of Lyn-SponGee and SponGee-Kras in distinct membrane compartments in retinal neurons by using membrane fractionation in a sucrose density gradient (Averaimo et al., 2016). Lyn-SponGee expression was restricted to low-density fractions, concomitant with the lipid raft marker Caveolin 1. In contrast, SponGee-Kras was enriched in the high-density fractions together with β-Adaptin, a marker of the non-raft component of the membrane (Figures 7C and 7D; Figure S4). To assess whether compartmentalization of SponGee differentially affects cGMP-dependent cellular responses, we analyzed the behavior of retinal ganglion cell growth cones expressing either Lyn-SponGee or SponGee-Kras when exposed to the axon guidance molecules slit1 and ephrinA5. Slit1- and ephrinA5-dependent repulsion of axonal growth cones require cGMP signaling (Nguyen-Ba-Charvet et al., 2001; Yue et al., 2008). The presence of a cGMP response in response to axon repellents was verified using ^{T}hPDE5^{VV} and ephrinA5 stimulation in retinal ganglion cell axons. EphrinA5 induces an elevation of cGMP that was blocked by SponGee (Figure S5). The biological response of axons expressing the soluble or targeted variants of SponGee and exposed to slit1 or ephrinA5 was evaluated to determine whether targeting SponGee to distinct subcellular compartments leads to differential axon behavior. In control conditions, including untransfected axons and mRFP-electroporated axons, slit1 and ephrinA5 induced the collapse of the growth cone (Figures 7E and 7F; Figure S6). SponGee expression in the cytosol abolished the collapse response induced by both cues, confirming the requirement of cGMP signaling in this process. Similarly, slit1 and ephrinA5 failed to induce growth cone collapse in Lyn-SponGee-expressing axons. In contrast, SponGee-Kras-expressing axons were indistinguishable from controls (Figures 7E and 7F; Figure S6), demonstrating that the blockade of cGMP signaling by SponGee in but not outside lipid rafts is sufficient to prevent slit1- and ephrinA5-induced growth cone collapse. Thus, targeting SponGee to distinct compartments enables the control of cGMP and its downstream signaling with subcellular resolution.

DISCUSSION

The present work introduces SponGee, a molecular scavenger of cGMP. We show that SponGee efficiently buffers cGMP, whereas

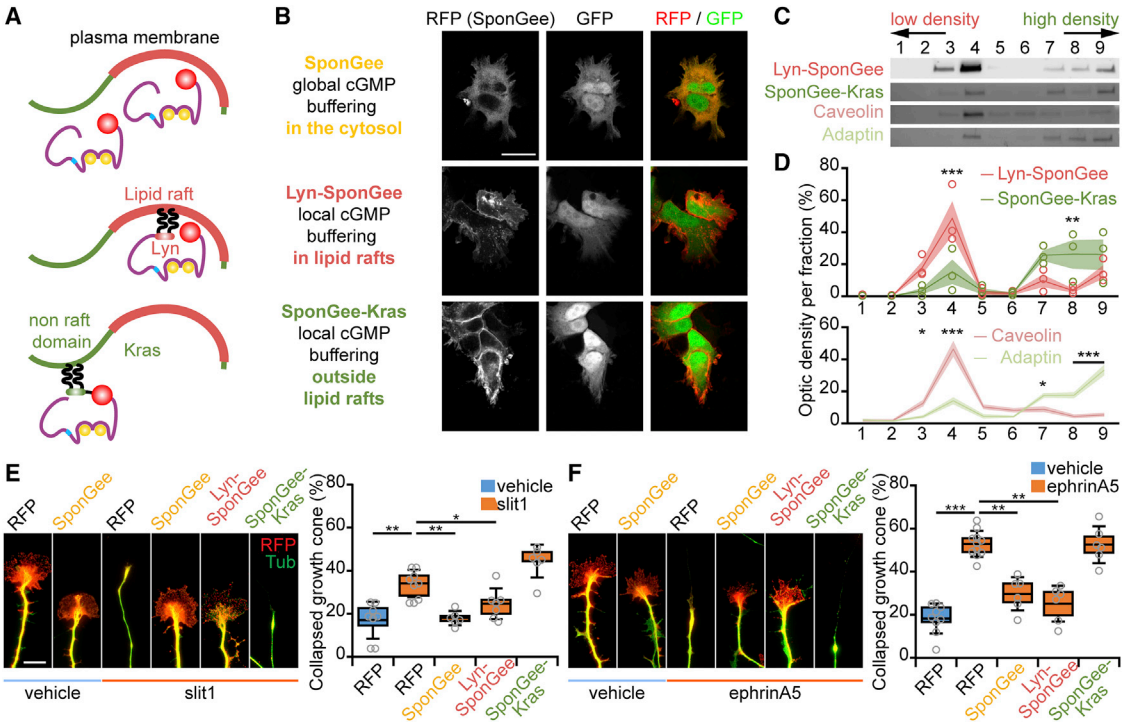

Figure 7. Subcellular Restriction of cGMP Manipulation Using SponGee

(A) SponGee was either used to alter cGMP signaling in the entire cell when not targeted to any cellular compartment or to prevent the activation of cGMP downstream effectors in specific compartments. Lyn-SponGee aims to be confined to lipid rafts whereas SponGee-Kras is intended to be restricted to the non-raft fraction of the plasma membrane.

(B) SponGee is detected in the cytoplasm (top row) whereas both Lyn-SponGee and SponGee-Kras are found at the plasma membrane (middle and bottom row).

(C) Plasma membrane fractionation highlights distinct subcellular localization of Lyn-SponGee and SponGee-Kras.

(D) Lyn-SponGee is highly enriched in fraction 4, whereas the localization of SponGee-Kras is shifted toward higher density fractions (7 to 9) (also see Figure S4).

(E and F) 200 ng·mL^{-1} slit1 (E) and (F) 500 ng·mL^{-1} ephrinA5 (F) induce growth cone collapse in control axons. SponGee and Lyn-SponGee prevents the collapse of growth cone. In contrast, SponGee-Kras does not affect axonal response to slit1 and ephrinA5 (also see Figures S6). Box-and-whisker plot elements: center line, mean; box limits, upper and lower quartiles; whiskers, SD.

Scale bars (B) 20 μM, (E) 10 μm. (C and D) *p < 0.05, **p < 0.01, ***p < 0.001; Two-way ANOVA followed by Bonferroni post hoc tests. (E and F) *p < 0.01, **p < 0.01, ***p < 0.001; Kruskal-Wallis test followed by Mann-Whitney post hoc tests. Exact p values and number of replicates are provided in Table S1.

See also Figures S4, S5, and S6.

it does not interact with the closely related cAMP. Because SponGee can be expressed in a subset of cells, the use of this cGMP buffer enables us to investigate the role of cGMP in cellular processes such as neuronal migration in a cell-specific manner. Furthermore, by including a high-affinity cGMP-binding domain of an endogenous protein, we have produced a specific and non-cytotoxic buffer that enables chronic manipulation of selected cell types. The possibility to target subcellular compartments further increases the ability of SponGee to affect a subset of cGMP-dependent downstream pathways with high specificity. Incidentally, ^{T}hPDE5^{VV}, the cGMP sensor introduced herein also offers the possibility to study cGMP modulation in cells, with more reversibility than the previously described cGi500.

Second messengers are key in the regulation of cellular responses to the environment and of their intrinsic behavior. Being able to manipulate the concentration of these signaling molecules in a precise and predictable fashion is crucial for the understanding of their downstream signaling cascades and cellular responses. Second messengers are situated at the convergence of multiple signaling cascades. A simple view of these signaling molecules diffusing freely in the cytosol conflicts the specific activation of each of their downstream effectors. The spatial confinement of second messengers emerged as a likely regulator of cellular responses (Augustine et al., 2003; Averaimo and Nicol, 2014; Averaimo et al., 2016). Much effort has been devoted to the development of tools that allow the subcellular manipulation of cAMP through genetically encoded tools (Averaimo et al., 2016; Lefkimmiatis et al., 2009) and calcium by using pharmacological agents targeting specific channels, but to date there is no refined way to block cGMP transients in a cell-dependent manner and with subcellular resolution. SponGee overcomes the issues of current cGMP manipulating methods by enabling both specificity for cGMP over cAMP and cellular selectivity when combined with cell-type specific promoters and subcellular localization when fused to known targeting sequences. It offers the possibility to investigate cGMP signals to a previously unachieved degree. SponGee also offers the opportunity to study the epistatic relationship between second

messengers in fields like axon guidance, where guidance molecules activating apparently the same signaling cascades are able to exert contradictive actions in developing axons (Akiyama et al., 2016; Nishiyama et al., 2003; Shelly et al., 2010).

SponGee was able to induce abnormalities in neuronal migration and axonal response to repellent cues and to compete with biosensors with an apparent EC_{50} of a few hundred nanomolar (^{T}hPDE5^{VV}, 320 nM; cGi500, 500 nM, Russwurm et al., 2007), which may seem contradictory with the described SponGee K_D obtained from overexpressing bacteria (0.97 μM). This apparent discrepancy might reflect the impact of expressing SponGee in *E. coli* rather than eukaryotic cells. SponGee folding or post-translational modifications might be affected in bacteria and that might reduce its ability to bind cGMP with high affinity. The use of SponGee as a cGMP scavenger in prokaryotic cells should be further validated. However, its ability to alter endogenous cGMP signaling in mouse and human cells has been extensively demonstrated here, suggesting that the affinity of SponGee for cGMP when expressed in eukaryotic cells might be higher in mammalian cells than when overexpressed in *E. coli*.

In the dawn of gene therapy, SponGee rises as a potential treatment for diseases characterized by overactivation of cGMP signaling pathways, such as retinitis pigmentosa (Huang et al., 1995; Vighi et al., 2018). Combining gene therapy with cellular and subcellular targeting strategies, SponGee offers an alternative approach enabling the specific manipulation of the abnormal pathways without altering other cGMP-dependent mechanisms. This targeted manipulation introduces cGMP as a therapeutic target with a limited risk of side effects.

In conclusion, SponGee has the potential to alter cGMP responses in a cell-specific manner and with subcellular resolution for the precise investigation of signaling cascades and opens new perspectives for specific therapeutic interventions.

STAR★METHODS

Detailed methods are provided in the online version of this paper and include the following:

- KEY RESOURCES TABLE
- LEAD CONTACT AND MATERIALS AVAILABILITY
- EXPERIMENTAL MODEL AND SUBJECT DETAILS
  - Animals
  - HEK293 Cell culture
- METHOD DETAILS
  - Molecular Biology
  - SponGee production and purification
  - Fluorescence anisotropy
  - Cell death assay
  - Rat hippocampal culture
  - EC_{50} and emission spectrum measurements
  - Membrane fractionation by detergent-free method
  - Immunoblotting
  - Expression of Guanylate Cyclases
  - Assessment of SponGee dimerization
  - VASP phosphorylation experiments
  - In utero electroporation
  - Collapse assay
  - Immunostaining
  - FRET Imaging and analysis (HEK293 cells)
  - FRET imaging (rat hippocampal cultures)
  - FRET data analysis (rat hippocampal culture)
  - Imaging of SponGee targeting
- QUANTIFICATION AND STATISTICAL ANALYSIS

SUPPLEMENTAL INFORMATION

Supplemental Information can be found online at https://doi.org/10.1016/j.celrep.2019.05.102.

ACKNOWLEDGMENTS

We are grateful to members of our labs and of J. Livet lab for thoughtful discussion, to P. Gaspar and N. Spitzer for helpful critical reading of the manuscript, to D. Koesling for the generous gift of cGi500, to K. Jalink for the generous gift of H147, to M. Sierksma for helpful insights in statistical analysis, and to the members of the animal and imaging facilities of Institut de la Vision. This work was supported by grants from Agence Nationale de la Recherche (ANR-15-CE16-0007-01), Retina France, and Sorbonne Université (FCS-SU IDEX SUPER SU-15-R-PERSU-17) to X.N. This work was performed in the frame of the LABEX LIFESENSES (ANR-10-LABX-65) and IHU FOReSIGHT (ANR-18-IAHU-0001), supported by French state funds managed by the Agence Nationale de la Recherche within the Investissements d'Avenir program. A.L. and S.B. were supported by a fellowship from the ED3C doctoral program (Sorbonne Université).

AUTHOR CONTRIBUTIONS

Conceptualization, X.N., Z.L., and O.R.; Methodology, X.N., O.R., Y.Z., K.L., A.A., Y.M., and Z.L.; Validation, X.N., O.R., K.L., and S.B.; Formal Analysis, X.N., O.R., S.R., D.L., Y.M., and Z.L.; Investigation, O.R., S.R., K.L., S.C., Y.Z., A.A., A.L., S.B., Y.M., and D.L.; Writing—Original Draft, O.R., K.L., and X.N.; Writing—Review and Editing, O.R., X.N., K.L., A.L., S.B., S.C., Y.Z., Y.M., and Z.L.; Visualization, O.R., D.L., and X.N.; Supervision, X.N., C.P., and Z.L.; Project Administration, X.N.; Funding Acquisition, X.N. and Z.L.

DECLARATION OF INTERESTS

A patent describing SponGee and its applications is pending.

Received: September 17, 2018
Revised: March 22, 2019
Accepted: May 29, 2019
Published: June 25, 2019

REFERENCES

Akiyama, H., Fukuda, T., Tojima, T., Nikolaev, V.O., and Kamiguchi, H. (2016). Cyclic Nucleotide Control of Microtubule Dynamics for Axon Guidance. J. Neurosci. *36*, 5636–5649.

Augustine, G.J., Santamaria, F., and Tanaka, K. (2003). Local calcium signaling in neurons. Neuron *40*, 331–346.

Averaimo, S., and Nicol, X. (2014). Intermingled cAMP, cGMP and calcium spatiotemporal dynamics in developing neuronal circuits. Front. Cell. Neurosci. *8*, 376.

Averaimo, S., Assali, A., Ros, O., Couvet, S., Zagar, Y., Genescu, I., Rebsam, A., and Nicol, X. (2016). A plasma membrane microdomain compartmentalizes ephrin-generated cAMP signals to prune developing retinal axon arbors. Nat. Commun. *7*, 12896.

Bhargava, Y., Hampden-Smith, K., Chachlaki, K., Wood, K.C., Vernon, J., Allerston, C.K., Batchelor, A.M., and Garthwaite, J. (2013). Improved genetically-encoded, FlincG-type fluorescent biosensors for neural cGMP imaging. Front. Mol. Neurosci. *6*, 26.

Brescia, M., and Zaccolo, M. (2016). Modulation of Compartmentalised Cyclic Nucleotide Signalling via Local Inhibition of Phosphodiesterase Activity. Int. J. Mol. Sci. *17*, E1672.

Castro, L.R., Verde, I., Cooper, D.M., and Fischmeister, R. (2006). Cyclic guanosine monophosphate compartmentation in rat cardiac myocytes. Circulation *113*, 2221–2228.

Depry, C., Allen, M.D., and Zhang, J. (2011). Visualization of PKA activity in plasma membrane microdomains. Mol. Biosyst. *7*, 52–58.

Gao, S., Nagpal, J., Schneider, M.W., Kozjak-Pavlovic, V., Nagel, G., and Gottschalk, A. (2015). Optogenetic manipulation of cGMP in cells and animals by the tightly light-regulated guanylyl-cyclase opsin CyclOp. Nat. Commun. *6*, 8046.

Gasser, C., Taiber, S., Yeh, C.-M., Wittig, C.H., Hegemann, P., Ryu, S., Wunder, F., and Möglich, A. (2014). Engineering of a red-light-activated human cAMP/cGMP-specific phosphodiesterase. Proc. Natl. Acad. Sci. USA *111*, 8803–8808.

Huang, S.H., Pittler, S.J., Huang, X., Oliveira, L., Berson, E.L., and Dryja, T.P. (1995). Autosomal recessive retinitis pigmentosa caused by mutations in the alpha subunit of rod cGMP phosphodiesterase. Nat. Genet. *11*, 468–471.

Huang, C.-C., Chan, S.H.H., and Hsu, K.-S. (2003). cGMP/protein kinase G-dependent potentiation of glutamatergic transmission induced by nitric oxide in immature rat rostral ventrolateral medulla neurons in vitro. Mol. Pharmacol. *64*, 521–532.

Kim, J.J., Lorenz, R., Arold, S.T., Reger, A.S., Sankaran, B., Casteel, D.E., Herberg, F.W., and Kim, C. (2016). Crystal Structure of PKG I:cGMP Complex Reveals a cGMP-Mediated Dimeric Interface that Facilitates cGMP-Induced Activation. Structure *24*, 710–720.

Klarenbeek, J.B., Goedhart, J., Hink, M.A., Gadella, T.W.J., and Jalink, K. (2011). A mTurquoise-based cAMP sensor for both FLIM and ratiometric read-out has improved dynamic range. PLoS One *6*, e19170.

Klarenbeek, J., Goedhart, J., van Batenburg, A., Groenewald, D., and Jalink, K. (2015). Fourth-generation epac-based FRET sensors for cAMP feature exceptional brightness, photostability and dynamic range: characterization of dedicated sensors for FLIM, for ratiometry and with high affinity. PLoS One *10*, e0122513.

Koch, K.-W., and Dell'Orco, D. (2015). Protein and Signaling Networks in Vertebrate Photoreceptor Cells. Front. Mol. Neurosci. *8*, 67.

Koesling, D., Mergia, E., and Russwurm, M. (2016). Physiological Functions of NO-Sensitive Guanylyl Cyclase Isoforms. Curr. Med. Chem. *23*, 2653–2665.

Kröner, C., Thunemann, M., Vollmer, S., Kinzer, M., Feil, R., and Richert, C. (2014). Endless: a purine-binding RNA motif that can be expressed in cells. Angew. Chem. Int. Ed. Engl. *53*, 9198–9202.

Kuhn, M. (2016). Molecular Physiology of Membrane Guanylyl Cyclase Receptors. Physiol. Rev. *96*, 751–804.

Lefkimmiatis, K., Moyer, M.P., Curci, S., and Hofer, A.M. (2009). "cAMP sponge": a buffer for cyclic adenosine 3′, 5′-monophosphate. PLoS One *4*, e7649.

Leterrier, C., Lainé, J., Darmon, M., Boudin, H., Rossier, J., and Lenkei, Z. (2006). Constitutive activation drives compartment-selective endocytosis and axonal targeting of type 1 cannabinoid receptors. J. Neurosci. *26*, 3141–3153.

Loulier, K., Lathia, J.D., Marthiens, V., Relucio, J., Mughal, M.R., Tang, S.-C., Coksaygan, T., Hall, P.E., Chigurupati, S., Patton, B., et al. (2009). beta1 integrin maintains integrity of the embryonic neocortical stem cell niche. PLoS Biol. *7*, e1000176.

Maag, D., and Lorsch, J.R. (2003). Communication between eukaryotic translation initiation factors 1 and 1A on the yeast small ribosomal subunit. J. Mol. Biol. *330*, 917–924.

Marden, J.N., Dong, Q., Roychowdhury, S., Berleman, J.E., and Bauer, C.E. (2011). Cyclic GMP controls Rhodospirillum centenum cyst development. Mol. Microbiol. *79*, 600–615.

Monestier, A., Lazennec-Schurdevin, C., Coureux, P.-D., Mechulam, Y., and Schmitt, E. (2018). Role of aIF1 in Pyrococcus abyssi translation initiation. Nucleic Acids Res. *46*, 11061–11074.

Mullershausen, F., Russwurm, M., Koesling, D., and Friebe, A. (2004). In vivo reconstitution of the negative feedback in nitric oxide/cGMP signaling: role of phosphodiesterase type 5 phosphorylation. Mol. Biol. Cell *15*, 4023–4030.

Nguyen-Ba-Charvet, K.T., Brose, K., Marillat, V., Sotelo, C., Tessier-Lavigne, M., and Chédotal, A. (2001). Sensory axon response to substrate-bound Slit2 is modulated by laminin and cyclic GMP. Mol. Cell. Neurosci. *17*, 1048–1058.

Nicol, X., Voyatzis, S., Muzerelle, A., Narboux-Nême, N., Südhof, T.C., Miles, R., and Gaspar, P. (2007). cAMP oscillations and retinal activity are permissive for ephrin signaling during the establishment of the retinotopic map. Nat. Neurosci. *10*, 340–347.

Nikolaev, V.O., Gambaryan, S., and Lohse, M.J. (2006). Fluorescent sensors for rapid monitoring of intracellular cGMP. Nat. Methods *3*, 23–25.

Nishiyama, M., Hoshino, A., Tsai, L., Henley, J.R., Goshima, Y., Tessier-Lavigne, M., Poo, M.-M., and Hong, K. (2003). Cyclic AMP/GMP-dependent modulation of Ca2+ channels sets the polarity of nerve growth-cone turning. Nature *423*, 990–995.

Pietrobon, M., Zamparo, I., Maritan, M., Franchi, S.A., Pozzan, T., and Lodovichi, C. (2011). Interplay among cGMP, cAMP, and Ca2+ in living olfactory sensory neurons in vitro and in vivo. J. Neurosci. *31*, 8395–8405.

Poppe, H., Rybalkin, S.D., Rehmann, H., Hinds, T.R., Tang, X.-B.B., Christensen, A.E., Schwede, F., Genieser, H.-G.G., Bos, J.L., Doskeland, S.O., et al. (2008). Cyclic nucleotide analogs as probes of signaling pathways. Nat. Methods *5*, 277–278.

Russwurm, M., Mullershausen, F., Friebe, A., Jäger, R., Russwurm, C., and Koesling, D. (2007). Design of fluorescence resonance energy transfer (FRET)-based cGMP indicators: a systematic approach. Biochem. J. *407*, 69–77.

Ruth, P., Pfeifer, A., Kamm, S., Klatt, P., Dostmann, W.R., and Hofmann, F. (1997). Identification of the amino acid sequences responsible for high affinity activation of cGMP kinase Ialpha. J. Biol. Chem. *272*, 10522–10528.

Ryu, M.-H., Moskvin, O.V., Siltberg-Liberles, J., and Gomelsky, M. (2010). Natural and engineered photoactivated nucleotidyl cyclases for optogenetic applications. J. Biol. Chem. *285*, 41501–41508.

Ryu, M.-H., Youn, H., Kang, I.-H., and Gomelsky, M. (2015). Identification of bacterial guanylate cyclases. Proteins *83*, 799–804.

Schneider, C.A., Rasband, W.S., and Eliceiri, K.W. (2012). NIH Image to ImageJ: 25 years of Image Analysis. Nat. Methods *9*, 671–675.

Shelly, M., Lim, B.K., Cancedda, L., Heilshorn, S.C., Gao, H., and Poo, M.M. (2010). Local and long-range reciprocal regulation of cAMP and cGMP in axon/dendrite formation. Science *327*, 547–552.

Stangherlin, A., Gesellchen, F., Zoccarato, A., Terrin, A., Fields, L.A., Berrera, M., Surdo, N.C., Craig, M.A., Smith, G., Hamilton, G., and Zaccolo, M. (2011). cGMP signals modulate cAMP levels in a compartment-specific manner to regulate catecholamine-dependent signaling in cardiac myocytes. Circ. Res. *108*, 929–939.

Vighi, E., Trifunović, D., Veiga-Crespo, P., Rentsch, A., Hoffmann, D., Sahaboglu, A., Strasser, T., Kulkarni, M., Bertolotti, E., van den Heuvel, A., et al. (2018). Combination of cGMP analogue and drug delivery system provides functional protection in hereditary retinal degeneration. Proc. Natl. Acad. Sci. USA *115*, E2997–E3006.

Weeks, K.M., and Crothers, D.M. (1992). RNA binding assays for Tat-derived peptides: implications for specificity. Biochemistry *31*, 10281–10287.

Wobst, J., von Ameln, S., Wolf, B., Wierer, M., Dang, T.A., Sager, H.B., Tennstedt, S., Hengstenberg, C., Koesling, D., Friebe, A., et al. (2016). Stimulators of the soluble guanylyl cyclase: promising functional insights from rare coding atherosclerosis-related GUCY1A3 variants. Basic Res. Cardiol. *111*, 51.

Yoshida, K., Tsunoda, S.P., Brown, L.S., and Kandori, H. (2017). A unique choanoflagellate enzyme rhodopsin exhibits light-dependent cyclic nucleotide phosphodiesterase activity. J. Biol. Chem. *292*, 7531–7541.

Yue, X., Dreyfus, C., Kong, T.A.-N., and Zhou, R. (2008). A subset of signal transduction pathways is required for hippocampal growth cone collapse induced by ephrin-A5. Dev. Neurobiol. *68*, 1269–1286.

Zaccolo, M., and Movsesian, M.A. (2007). cAMP and cGMP signaling cross-talk: role of phosphodiesterases and implications for cardiac pathophysiology. Circ. Res. *100*, 1569–1578.

Zacharias, D.A., Violin, J.D., Newton, A.C., and Tsien, R.Y. (2002). Partitioning of lipid-modified monomeric GFPs into membrane microdomains of live cells. Science *296*, 913–916.

STAR★METHODS

KEY RESOURCES TABLE

REAGENT or RESOURCE	SOURCE	IDENTIFIER
Antibodies		
Cleaved Caspase 3 (Asp175)	Cell Signaling	Cat# 9661S, lot # 0043. RRID: AB_2341188.
Mouse anti-α-tubulin	Sigma-Aldrich	Cat# T6199, lot # 024M4850V. RRID: AB_477583.
Rabbit anti-β-adaptin (H-300)	Santa Cruz Biotechnology	Cat# sc-10762, lot # E1304. RRID: AB_2242872
Living Colors® DsRed Polyclonal Antibody	Clontech	Cat# 632496, lot # 1306037. RRID: AB_10013483
Rabbit Anti-Caveolin Polyclonal Antibody	BD Biosciences	Cat# 610060, lot # GR256941. RRID: AB_397472
GUCY1A3 Monoclonal Antibody (3G6B2)	Thermo Fisher Scientific	Cat# MA5-17086, lot # TJ2659608. RRID: AB_2538557
GUCY1B3 Polyclonal Antibody	Thermo Fisher Scientific	Cat# PA5-42803, lot # TJ2266011. RRID: AB_2608158
Phospho-VASP (Ser239) Antibody	Cell Signaling Technology	Cat# 3114, lot # 7. RRID: AB_2213396
VASP (9A2) Rabbit mAb antibody	Cell Signaling Technology	Cat#3132, lot # 4. RRID: AB_2213393
GFP Tag Polyclonal Antibody	Thermo Fisher Scientific	Cat# A11122, lot # 1789911. RRID: AB_221569
Peroxidase-AffiniPure Goat Anti-Rabbit IgG (H+L) antibody	Jackson ImmunoResearch Labs	Cat# 111-035-003, lot # 81283. RRID: AB_2313567
Peroxidase-AffiniPure Goat Anti-Mouse IgG (H + L) antibody	Jackson ImmunoResearch Labs	Cat# 115-035-003. RRID: AB_10015289
Donkey Anti-Mouse IgG (H+L) Antibody, Alexa Fluor 488 Conjugated	Thermo Fisher Scientific	Cat# A21202, lot # 1562298. RRID: AB_141607
Donkey anti-Rabbit IgG (H+L) Highly Cross-Adsorbed Secondary Antibody, Alexa Fluor 594	Thermo Fisher Scientific	Cat# A21207, lot # 1602780. RRID: AB_141637
Critical Commercial Assays		
CellEvent Caspase-3/7 Green Detection Reagent	Thermo Fisher Scientific	Cat# C10723, lot # 1932830. RRID: Not available
Experimental Models: Cell Lines		
HEK293	ATCC	Cat# CRL-1573. RRID: CVCL_0045
Experimental Models: Organisms/Strains		
Mus musculus C57BL/6JRj	Janvier Labs	RRID:MGI:2670020
Mus musculus RjOrl:SWISS	Janvier Labs	RRID:MGI:2168141
Recombinant DNA		
SponGee	This Paper	N/A
Lyn-SponGee	This Paper	N/A
SponGee-Kras	This Paper	N/A
^{T}hPDE5^{vv}	This Paper	N/A
cGi500	Russwurm et al., 2007	N/A
Software and Algorithms		
ImageJ	Schneider et al., 2012	https://imagej.nih.gov/ij/ RRID:SCR_003070
GraphPad Prism	GraphPad Software Inc.	RRID:SCR_002798

LEAD CONTACT AND MATERIALS AVAILABILITY

Further information and requests for resources and reagents should be directed to and will be fulfilled by the Lead Contact, Xavier Nicol (xavier.nicol@inserm.fr).

EXPERIMENTAL MODEL AND SUBJECT DETAILS

Animals

Pregnant C57BL6/J and RjOrl:SWISS mice and Sprague–Dawley rats were purchased from Janvier Labs. All animal procedures were performed in accordance with institutional guidelines and approved by local ethics committees (C57BL6/J mice, C2EA-05: Comité

d'éthique en expérimentation animale Charles Darwin; Sprague–Dawley rats, ethics committee C2EA-59: Comité d'éthique en matière d'expérimentation animale Paris Centre et Sud). Animals were housed under 12 h light/12 h dark cycle. Embryos from dated matings (developmental stage stated in each section describing individual experiments) were not sexed during the experiments and the female over male ratio is expected to be close to 1.

HEK293 Cell culture

HEK293T cells (ATCC, not authenticated, free of mycoplasma contamination) were kept in a 37°C, 5% CO2 incubator and transfected using Lipofectamine 2000 (Life Technologies) according to the manufacturer's protocol and imaged the day following transfection or fixed and processed for immunocytofluorescence.

METHOD DETAILS

Molecular Biology

SponGee (5′-ATGAGCGAGCTGGAGGAAGACTTTGCCAAGATTCTCATGCTCAAGGAGGAGAGGATCAAAGAGCTGGAGAAGCGG
CTGTCAGAGAAGGAGGAAGAAATCCAGGAGCTGAAGAGGAAACTCCATAAATGCCAGTCAGTGCTGCCCGTGCCCTCGACCCAC
ATCGGCCCCCGGACCACCCGGGCACAGGGCATCTCGGCCGAGCCGCAGACCTACAGGTCCTTCCACGACCTCCGAGTGACCC
TGCCCTTCTACCCCAAGAGTCCACAGTCCAAGATCGATCTCATAAAGGAGGCCATCCTTGACAATGACTTTATGAAGAACTTGGAG
CTGTCACAGATCCAAGAGATTGTGGATTGTATGTACCCAGTGGAGTACGGCAAAGACAGCTGCATCATCAAAGAAGGAGATGTGG
GGTCACTGGTGTATGTCATGGAAGATGGTAAGGTTGAAGTTACAAAAGAAGGCGTGAAGCTGTGCACAATGGGTCCTGGTAAAGT
GTTTGGAGAGTTGGCTATCCTTTACAACTGTACCCGGACGGCGACCGTCAAAACTCTTGTAAATGTGAAACTCTGGGCCATTGATC
GACAATGTTTTCAGACGATAATGATGAGGACAGGACTTATCAAGCATACCGAGTATATGGAATTTTTAAAAAGCGTTCCAACATTCC
AGAGCCTTCCTGAAGAGATCCTCAGTAAACTTGCTGACGTCCTTGAAGAGACCCACTATGAAAATGGGGAATATATCATCAGGCAA
GGTGCAAGAGGGGACACCTTCTTTATCATCAGTAAAGGAAAGGTTAATGTCACTCGTGAAGACTCGCCCAATGAAGACCCAGTCT
TTCTTAGAACCTTAGGAAAAGGAGATTGGTTTGGAGAGAAAGCCTTGCAGGGGGAAGATGTGAGAACAGCGAATGTAATTGCGGC
AGAAGCTGTAACCTGCCTTGTGATCGACAGAGACTCTTTCAAACATTTGATTGGAGGATTAGATGATGTTTCTAATAAAGCATATGA
AGATGCAGAAGCTAAG-3′) was designed *in silico* in frame with a tandem repeat of the Lyn Kinase N-terminal domain (5′-ATGG
GCTGCATCAAGAGCAAGCGCAAGGACAAGATGGGCTGCATCAAGAGCAAGCGCAAGGACAAG-3′) and FLAG tag in 5′ of SponGee, and the desired sequences obtained as oligonucleotides from Sigma and Life Technologies, respectively. The oligos were annealed and cloned into pcDNA3-mRFP in frame with the reporter sequence. Lipid-raft-excluded and cytosolic forms of the SponGee variants were obtained by subcloning into pcDNA3 with or without the CaaX-polylysine motif of Kras (5′-CAAGAAGAA
GAAGAAGAAGAAGAGCAAGA'), respectively. For expression on RGCs, the constructs were subcloned into pCX.

The sequence of the truncated human PDE5A1 (hPDE5) was obtained by gene synthesis in the pUC57 vector (Genscript) and digested with SmaI and NheI enzymes (New England Biolabs). The Epac1 sequence was removed from the ^{T}Epac^{VV} vector (obtained from Dr Kees Jalink, NKI-AVL, Amsterdam, Netherlands) by digestion with EcoRV and NheI (New England Biolabs) and replaced by hPDE5. The resulting final sequence of ^{T}hPDE5^{VV} is ATGGTGAGCAAGGGCGAGGAGCTGTTCACCGGGGTGGTGCCCATCC
TGGTCGAGCTGGACGGCGACGTAAACGGCCACAAGTTCAGCGTGTCCGGCGAGGGCGAGGGCGATGCCACCTACGGCAAGCT
GACCCTGAAGTTCATCTGCACCACCGGCAAGCTGCCCGTGCCCTGGCCCACCCTCGTGACCACCCTGTCCTGGGGCGTGCAGT
GCTTCGCCCGCTACCCCGACCACATGAAGCAGCACGACTTCTTCAAGTCCGCCATGCCCGAAGGCTACGTCCAGGAGCGCACCA
TCTTCTTCAAGGACGACGGCAACTACAAGACCCGCGCCGAGGTGAAGTTCGAGGGCGACACCCTGGTGAACCGCATCGAGCTGA
AGGGCATCGACTTCAAGGAGGACGGCAACATCCTGGGGCACAAGCTGGAGTACAACTACATCAGCGACAACGTCTATATCACCG
CCGACAAGCAGAAGAACGGCATCAAGGCCAACTTCAAGATCCGCCACAACATCGAGGACGGCGGCGTGCAGCTCGCCGACCAC
TACCAGCAGAACACCCCCATCGGCGACGGCCCCGTGCTGCTGCCCGACAACCACTACCTGAGCACCCAGTCCAAGCTGAGCAA
AGACCCCAACGAGAAGCGCGATCACATGGTCCTGCTGGAGTTCGTGACCGCCGCCCGATGGGAATTAGTGAAGGATATTTCTAG
TCATTTGGATGTCACAGCCTTATGTCACAAAATTTTCTTGCATATCCATGGACTGATATCTGCTGACCGCTATTCCCTGTTCCTTGTCT
GTGAAGACAGCTCCAATGACAAGTTTCTTATCAGCCGCCTCTTTGATGTTGCTGAAGGTTCAACACTGGAAGAAGTTTCAAATAAC
TGTATCCGCTTAGAATGGAACAAAGGCATTGTGGGACATGTGGCAGCGCTTGGTGAGCCCTTGAACATCAAAGATGCATATGAGG
ATCCTCGGTTCAATGCAGAAGTTGACCAAATTACAGGCTACAAGACACAAAGCATTCTTTGTATGCCAATTAAGAATCATAGGGAAG
AGGTTGTTGGTGTAGCCCAGGCCATCAACAAGAAATCAGGAAACGGTGGGACATTTACTGAAAAAGATGAAAAGGACTTTGCTG
CTTATTTGGCAGCTAGCGAGCTCATGGACGGCGGCGTGCAGCTCGCCGACCACTACCAGCAGAACACCCCCATCGGCGACGGC
CCCGTGCTGCTGCCCGACAACCACTACCTGAGCTACCAGTCCGCCCTGAGCAAAGACCCCAACGAGAAGCGCGATCACATGGT
CCTGCTGGAGTTCGTGACCGCCGCCGGGATCACTCTCGGCATGGACGAGCTGTACAAGGGTGGCAGCGGTGGCATGGTGAGCA
AGGGCGAGGAGCTGTTCACCGGGGTGGTGCCCATCCTGGTCGAGCTGGACGGCGACGTAAACGGCCACAAGTTCAGCGTGT
CCGGCGAGGGCGAGGGCGATGCCACCTACGGCAAGCTGACCCTGAAGCTGATCTGCACCACCGGCAAGCTGCCCGTGCCCTGGC
CCACCCTCGTGACCACCCTGGGCTACGGCCTGCAGTGCTTCGCCCGCTACCCCGACCACATGAAGCAGCACGACTTCTTCAAGT
CCGCCATGCCCGAAGGCTACGTCCAGGAGCGCACCATCTTCTTCAAGGACGACGGCAACTACAAGACCCGCGCCGAGGTGAAG
TTCGAGGGCGACACCCTGGTGAACCGCATCGAGCTGAAGGGCATCGACTTCAAGGAGGACGGCAACATCCTGGGGCACAAGCT
GGAGTACAACTACAACAGCCACAACGTCTATATCACCGCCGACAAGCAGAAGAACGGCATCAAGGCCAACTTCAAGATCCGCCA
CAACATCGAGCCGAATTTTGTCTTCCTGATCGGCGCCGCAGGAATACTCTTCGTATCTAGCGAGCTCATGGTGAGCAAGGGCGAG

GAGCTGTTCACCGGGGTGGTGCCCATCCTGGTCGAGCTGGACGGCGACGTAAACGGCCACAAGTTCAGCGTGTCCGGCGAGG
GCGAGGGCGATGCCACCTACGGCAAGCTGACCCTGAAGCTGATCTGCACCACCGGCAAGCTGCCCGTGCCCTGGCCCACCCT
CGTGACCACTCTGGGCTACGGCCTACAGTGCTTCGCCCGCTACCCCGACCACATGAAGCAGCACGACTTCTTCAAGTCCGCCAT
GCCCGAAGGCTACGTCCAGGAGCGCACCATCTTCTTCAAGGACGACGGCAACTACAAGACCCGCGCCGAGGTGAAGTTCGAGG
GCGACACCCTGGTGAACCGCATCGAGCTGAAGGGCATCGACTTCAAGGAGGACGGCAACATCCTGGGGCACAAGCTGGAGTAC
AACTACAACAGCCACAACGTCTATATCACCGCCGACAAGCAGAAGAACGGCATCAAGGCCAACTTCAAGATCCGCCACAACATCG
AGGACGGCGGCGTGCAGCTCGCCGACCACTACCAGCAGAACACCCCCATCGGCGACGGCCCCGTGCTGCTGCCCGACAACCA
CTACCTGAGCTACCAGTCCGCCCTGAGCAAAGACCCCAACGAGAAGCGCGATCACATGGTCCTGCTGGAGTTCGTGACCGCCGC
CGGGATCACTCTCGGCATGGACGAGCTGTACAAGCCGAATTCCCTCGAGGTTAACGCGGCGCGCCTCTAA.

SponGee production and purification

The full-length SponGee cDNA was subcloned into a pEXP5-NT/TOPO vector (Invitrogen V960-05) in frame with the N-terminal peptide containing a polyhistidine (6xHis) tag. Protein was produced in Bl21-CodonPlus (DE3)-RIPL competent cells (Agilent technologies 230280). The His-tagged recombinant protein was purified using a Ni-NTA (nickel-nitrilotriacetic acid) column. It was then eluted in a buffer containing 30 mM MOPS (3-Morpholinopropanesulfonic acid), pH 7.2 and 200 mM NaCl. Protein concentration was deduced from A_{280} measurement using a computed extinction coefficient of 5500 M^{-1} cm^{-1}.

Fluorescence anisotropy

The dissociation constant of fluorescein-labeled cGMP (Fluo-cGMP) was measured using fluorescence anisotropy experiments essentially as described (Kim et al., 2016). Fluo-cGMP was diluted to 3.2 nM in a final volume of 300 μL in a buffer containing 30 mM MOPS-HCl (pH 7.2), 300 mM NaCl. All measurements were performed in a Hellma 1 cm x 0.4 cm cuve at 37°C with a FP-8300 JASCO spectrofluorometer. Fluorescence anisotropy (r) was recorded at 530 nm (λ_{exc} = 485 nm). Aliquots of SPG (0.1 to 4.4 μM) were added for titration. For each titration point, 10 anisotropy measurements were recorded successively at different times in order to verify that equilibrium has been reached. Dissociation constant was calculated from simple binding curves by non-linear regression using Origin (OriginLab Corp., Northampton, USA), assuming one site per monomer. Results are the average ± sd from 3 independent experiments.

For the measurement of the dissociation constant of cGMP, competition experiments were performed. Samples containing 3.2 nM Fluo-cGMP (Biolog) and 2 μM SponGee were titrated with unlabeled. Fluorescence anisotropy was plotted as a function of cGMP concentration and fitted as described (Maag and Lorsch, 2003; Monestier et al., 2018) by non-linear regression (Origin, OriginLab Corp., Northampton, USA) using a quadratic equation (Weeks and Crothers, 1992).

$$r = r_{FcGMP} + [r_{SpG:FcGMP} - r_{FcGMP}] \times \frac{\left([KL] + \frac{KL[cGMP]}{KU} + [SpG] + [FcGMP]\right) - \sqrt{(KL + KL[cGMP]/KU + [SpG] + [FcGMP])^2 - 4[FcGMP][SpG]}}{2[FcGMP]}$$

where [FcGMP] is the total concentration of fluorescent cGMP, [SpG] is the concentration of SponGee, KL is the dissociation constant of F-cGMP from its complex with SponGee, [cGMP] is the concentration of unlabeled cGMP, KU is the dissociation constant of cGMP from its complex with SponGee, r_{FcGMP} is the fluorescence anisotropy of Fluo-cGMP and $r_{SpG:FcGMP}$ is the fluorescence anisotropy of the SPG:F-cGMP complex. For all titrations, it was verified that fluorescence emission did not change upon binding and therefore no correction for changes in quantum yield have been performed. Results are the average ± sd from 3 independent experiments.

Cell death assay

HEK293 Cells were plated on poly-lysine-coated coverslips and transfected the next day with a pCX-mRFP or a pCX-SponGee vector using Lipofectamine 2000 (Thermo Fisher) following the manufacturer's instructions. Three days after plating, cells were either fixed with 4% paraformaldehyde and processed for immunocytochemistry with the antibodies against Cleaved Caspase 3 (Asp175; Cell Signaling; lot # 0043) and α-tubulin (Sigma) or treated with the CellEvent Caspase 3/7 Green Detection Reagent (Thermo Fisher) for 30 min and then fixed and labeled with an α-tubulin antibody. For each experiment, the proportion of Caspase3-positive over unlabeled cells in the population of mRFP- or SponGee-positive cells was computed from 10 randomly chosen fields acquired on a 20x air objective in a DM6000 microscope (Leica Microsystems).

Rat hippocampal culture

Hippocampal neuronal cultures were performed essentially as described previously (Leterrier et al., 2006). Briefly, hippocampi of rat embryos were dissected at embryonic day 18. After trypsinization, dissociation was achieved with a fire-polished Pasteur pipette. Cells were counted and plated on poly-D-lysine-coated 18-mm diameter glass coverslips, at a density of 300–400 cells·mm^{-2}. The plating medium was Neurobasal (Life Technologies) supplemented with 2% B27 (Life Technologies) and containing stabilized Glutamine (0.5 mM) and penicillin G (10 U·mL^{-1})/streptomycin (10 g·mL^{-1}). Four h after plating, the coverslips were transferred

into Petri dishes containing supplemented Neurobasal medium that had been conditioned for 24 h on an 80% confluent glia layer. Neurons were transfected after 6 days *in vitro* (DIV) using Lipofectamine 2000 (Life Technologies), following the manufacturer's instructions.

EC_{50} and emission spectrum measurements

Cells transfected with ^{T}hPDE5^{VV} were washed thrice with ice cold PBS and collected in 5mM Tris-HCL, 2 mM EGTA, pH = 7.3. Cells were sonicated during 45 s on ice with a Vibra-Cell (Bioblock Scientific). Lysates were pelleted and the emission of the supernatants was imaged with an Infinite M1000 plate reader and the software Magellan 7.2 SP1 (Tecan). For spectral emission the samples were excited at 434/10 nm, and the emissions analyzed from 450 to 600 nm with 2nm increments, in absence or presence (200 μM). Samples were mixed with standardized dilutions of cAMP and cGMP (Biolog) and the ratio of emissions at 480 nm over 540 nm was used to calculate the EC_{50} of the sensor in GraphPad Prism (GraphPad Software Inc.).

Membrane fractionation by detergent-free method

Membrane fractionation was performed as described previously (Averaimo et al., 2016). Electroporated retinas were pelleted (195 g for 5 min at 4°C) and resuspended in 1.34 mL of 0.5 M sodium carbonate, pH 11.5, with protease inhibitor cocktail and phosphatase inhibitor cocktail 1, 2 and 3 (Sigma-Aldrich). The homogenate was sheared through a 26-gauge needle and sonicated three times for 20 s bursts. The homogenate was adjusted to 40% sucrose by adding 2.06 mL of 60% sucrose in MBS (25 mM MES, pH 6.4, 150 mM NaCl, and 250 mM sodium carbonate), placed under a 5%–30% discontinuous sucrose gradient, and centrifuged at 34,000 rpm for 15–18 h at 4°C in a Beckman SW 41Ti rotor. Nine fractions (1.24 mL each) were harvested from the top of the tube, mixed with 9 volumes of MBS, and centrifuged at 40,000 rpm for 1 h at 4°C (Beckman SW-41Ti rotor). Supernatants were discarded, and membrane pellets were resuspended in 100 μl of 1% SDS.

Immunoblotting

For immunoblotting, samples were separated on 4%–15% Mini- Protean TGX Tris-Glycine-buffer SDS-PAGE (Biorad) and transferred onto 0.2 μm Trans-Blot Turbo nitrocellulose membranes (Biorad). Membranes were blocked for 1 h at room temperature in 1xTBS (10 mM Tris pH 8.0, 150 mM NaCl,) supplemented with 5% (w/v) dried skim milk powder. Primary antibody incubation was carried out overnight at 4°C, with the following antibodies: rabbit anti-DsRed (1/200; 632476; Clontech; lot # 1306037), rabbit anti-β-Adaptin (1/200; sc-10762; Santa Cruz; lot # E1304) and rabbit anti-Caveolin (1/500; 610060; BD Transduction Laboratories; lot # GR256941). All primary antibodies have been previously validated for this assay (Averaimo et al., 2016). A goat anti-rabbit-HRP coupled secondary antibody was used for detection (Jackson ImmunoResearch, West Grove, PA). After antibody incubations, membranes were extensively washed in TBS T (TBS containing 2.5% Tween-20). Western blots were visualized using the enhanced chemiluminescence method (ECL prime Western Blotting detection reagent, Amersham).

Expression of Guanylate Cyclases

In order to evaluate the endogenous expression of sGCs in HEK293T cells, total cellular proteins were extracted in lysis buffer (10mM HEPES pH 7, 100 mM NaCl, 2 mM EDTA, 0.5% NP-40) supplemented with protease inhibitor cocktail and phosphatase inhibitor cocktails 1 and 3 (Sigma-Aldrich). Proteins were separated, transferred, incubated with mouse anti-GUCY1A3 (1/500; MA5-17086; Thermofisher Scientific; lot # TJ2659608) or rabbit anti-GUCY1B3 (1/500; PA5-42803; Thermofisher Scientific; lot # TJ266011) antibodies and visualized as described above using goat anti-mouse or goat anti-rabbit HRP as secondary antibodies and ECL Prime for the detection.

Assessment of SponGee dimerization

To explore the possibility of expression of Spongee as monomers or dimers, cellular extracts of HEK293T cells expressing SponGee were analyzed by SDS-PAGE under non-reducing (DTT free) or reducing condition (addition of 5 mM DTT) then transferred and incubated with rabbit anti-DsRed antibody (1/200; 632496; Clontech; lot # 1306037) and revealed as described before.

VASP phosphorylation experiments

For phosphorylation studies, HEK293T cells were transfected or not with SponGee vectors for 24 h after plating using Lipofectamine 2000 according to the manufacturer's instructions (Invitrogen). For stimulation, cells were incubated for 5 min with 50 μM Spermine-NONOate or vehicle at 37°C in the presence or not of ODQ. In this case, 30 min before stimulation with Spermine-NONOate, vehicle solution or ODQ 100μM (R&D Systems) was applied. NO stimulation reaction was stopped by placing cells on ice followed by extraction of proteins described before. Samples were then separated and membranes incubated with rabbit anti-phospho-VASP (Ser239) (1/500; 3114; Cell Signaling; lot # 7) or rabbit anti-VASP (1/500; 3132. Cell Signaling; lot # 4) and visualized with goat anti-rabbit HRP as secondary antibodies and ECL Prime for the detection.

In utero electroporation

Timed pregnant females (Janvier Labs) were delivered to the animal facility a week prior to the surgery in order to allow a minimum of 5-days adaptation. In utero electroporation was performed as described previously (Loulier et al., 2009). E14.5 females were

anesthetized with Ketamine/Xylazine and a midline laparotomy was performed, exposing uterine horns and allowing visualization of embryos under oblique illumination. 1 μL of DNA containing two plasmids vectors combined 3:1 with sterile Fast Green dye (Sigma) was injected with a glass capillary pipette (75–125 μm outer diameter with beveled tip) driven by a INJECT+MATIC (INJECT+MATIC) microinjector into the lateral ventricle of each embryo. Two different plasmid vectors were injected simultaneously. The first was a plasmid encoding green fluorescent protein under the control of the chicken beta actin promoter (pCX-eGFP), used as a control of electroporation. The second was either a plasmid encoding red fluorescent protein (mRFP) control construct or SponGee-mRFP. The anode of 5 mm diameter tweezertrodes (Sonidel Limited) was placed above the dorsal telencephalon and four 35-V pulses of 50 ms duration were applied across the uterine sac. Following intrauterine surgery, the incision site was closed with sutures (4-0, Ethicon) and the mouse was allowed to recover in a clean cage. Mice were either euthanized 4 days after surgery to harvest E18.5 embryonic brains, or allowed to give birth for analysis at P10 postnatal stage. Embryonic brains were dissected out, immersed overnight in Antigenfix (Diapath) fixative solution and rinsed in PBS prior to sectioning. P10 mice were deeply anesthetized with sodium pentobarbital (150 $mg \cdot kg^{-1}$), perfused transcardially with Antigenfix (Diapath), brains dissected out and postfixed overnight in the same solution. Embryonic and postnatal brain samples were sectioned at 200 μm thickness on a vibrating blade microtome (Leica VT 1000S). Finally, sections were either mounted in Vectashield+Dapi (Vector laboratories) or incubated 2 h in 10 $\mu g \cdot mL^{-1}$ bis-benzimide (Sigma Aldrich) and mounted in Mowiol 4-88 (Sigma Aldrich). Confocal images were acquired with a 60X oil-immersion objective (N.A. 1.4) and a Z stack containing the whole specimen was sampled at Nyquist frequency in an Olympus FV1000 confocal microscope. Images were rendered in ImageJ and Photoshop.

Collapse assay

Retinas of E14 mouse embryos were electroporated with mRFP, Lyn-SponGee, SponGee or SponGee-Kras using two poring pulses (square wave, 175V, 5ms duration, with 50ms interval) followed by four transfer pulses (40V, 50 ms duration and 950 ms interpulse interval) with a Nepa21 Super Electroporator (NepaGene). Retinas were dissected and kept 24 h in culture medium (DMEM-F12 supplemented with glutamine (Sigma Aldrich), penicillin/streptomicin (Sigma Aldrich), BSA (Sigma Aldrich) and glucose, in a humidified incubator at 37°C and 5% CO2. The day after, they were cut into 200 μm squares with a Tissue-Chopper (McIlwan) and explants were plated on glass coverslips coated with poly- lysine and Laminin (Sigma Aldrich). Cells were cultured for 24 h in culture medium supplemented with 0.4% methyl cellulose and B-27 (Life Technologies) and treated with 200 $ng \cdot mL^{-1}$ rmSlit1 or 500 $ng \cdot mL^{-1}$ rmEphrinA5 (R&D Systems) for 1 h.

Immunostaining

Retinal explants, or HEK cells coexpressing the targeted versions of SponGee and GFP, were fixed with 4% PFA in PB for 30 min, permeabilized and blocked and with 1% Triton and 3% BSA in PBS, then incubated with antibodies against DsRed (632496, Clontech, lot # 1306037, previously used in a similar assay, (Averaimo et al., 2016) followed by a secondary antibody coupled to AlexaFluor 594 (A21207, Life Technologies, lot # 1602780) and GFP (A11122, Life Technologies, lot # 1789911, previously validated in Nicol et al., 2007) or α-Tubulin (T6199, Sigma, lot # 024M4850V, previously validated in Nicol et al., 2007) followed by a secondary antibody coupled to AlexaFluor 488 (A21202, Life Technologies, lot # 1562298).

FRET Imaging and analysis (HEK293 cells)

Images were acquired with an inverted DMI6000B epifluorescence microscope (Leica) coupled to a 40x oil-immersion objective (N.A. 1.3) and the software Metamorph (Molecular Devices). For live imaging experiments, cells transfected with ^{T}hPDE5^{VV} or H147, and co-expressing mRFP or SponGee were perfused with 1 mM $CaCl_2$, 0.3 μM $MgCl_2$, 0.5 mM Na_2HPO_4, 0.5 mM NaH_2PO_4, 0.4 μM $MgSO_4$, 4.25 mM KCl, 14 μM $NaHCO_3$, 120 mM NaCl, 0.0004% $CuSO_4$, 1.24 μM Fe $(NO_3)_3$, 1.5 μM $FeSO_4$, 1.5 μM thymidine, 0.51 mM lipoic acid, 1.5 mM $ZnSO_4$, 0.5 μM sodium pyruvate (all from Sigma), 1X MEM Amino Acids (Life Technologies), 1X non-essential amino acids (Life Technologies), 25 mM HEPES (Sigma), 0.5 mM putrescine (Sigma), 0.01% BSA (Sigma), 0.46% glucose (Sigma), 1 mM glutamine (Life Technologies), 2% penicillin/streptomicin (Life Technologies). Vitamin B12 and riboflavin were omitted because of their autofluorescence. Spermine-NONOate was used at 50 μM (in the range of previous use, Huang et al., 2003), ODQ (Tocris) at 10 μM, or at 100 μM when used in experiments where NO was to be used, and Forskolin (Sigma) at 10 μM. Images were acquired simultaneously for the CFP (483/32 nm) and YFP (542/27) channels every 20 s while cells were continuously superfused with the medium described above. Simultaneous CFP and YFP channel acquisition was achieved using a dual chip CCD camera -D2 (Hamamatsu). The wavelength used for CFP excitation in HEK cells was 436/20 nm. Images were processed in ImageJ, corrected for background and bleedthrough from CFP into the YFP channel. The ratio YFP:CFP (^{T}hPDE5^{VV}) or CFP:YFP (H147 and cGI500) was computed and normalized to the initial values for each single cell.

FRET imaging (rat hippocampal cultures)

Neurons transfected with ^{T}hPDE5^{VV} probe were imaged by videomicroscopy between DIV8 and DIV11 on a motorized Nikon Eclipse Ti-E/B inverted microscope with the Perfect Focus System (PFS) in a 37°C thermostated chamber, using an oil immersion CFI Plan APO VC 60x, NA 1.4 objective (Nikon). Acquisitions were carried out at the excitation wavelength of the CFP (434nm ± 15nm) using an Intensilight (Nikon). Emitted light passed through an Optosplit II beam-splitter (Cairn Research) equipped with a FF509-FDi01 dichroïc mirror, a FF01-483/32-25 CFP filter and a FF01-542/27-25 YFP filter and was collected by an EM-CCD camera (Evolve 512,

Photometrics), mounted behind a 2x magnification lens. Acquisitions were performed by piloting the set-up with Metamorph 7.7 (Molecular Devices). All filter sets were purchased from Semrock. Cultured neurons on 18-mm coverslips were placed in a closed imaging chamber containing an imaging medium: 120 mM NaCl, 3 mM KCl, 10 mM HEPES, 2 mM $CaCl_2$, 2 mM $MgCl_2$, 10 mM D-glucose, 2% B27, 0,001% BSA. The acquisition lasted 70 min registering one image every 2 min, registering in parallel 4 to 6 neurons on the same coverslip. 30 min after the beginning of the acquisition, vehicle solution or ODQ 100 μM (R&D Systems) was applied 40 min after the onset of acquisition, DEA NONOate (Sigma) 50μM or Forskolin (Sigma) 10μM was applied.

FRET data analysis (rat hippocampal culture)

Images were divided in two parts on ImageJ to separate the CFP channel from the YFP channel. Data were then analyzed on MATLAB by calculating the FRET ratio at each time point for one or several Regions Of Interest (ROIs). The user defined ROIs for each position. For each image, the value of the FRET ratio corresponds to$(IY - BY/IC - BC)$, where IY is the mean intensity of the ROI in the YFP channel; BY is the mean intensity of the background in the YFP channel; IC is the mean intensity of the ROI in the CFP channel; BC is the value of the background in the CFP channel. For each ROI, the FRET ratio was then normalized by the baseline mean, defined as the 7 time points before first treatment injection. FRET Ratio $= 100 * (Rc - Ro/Ro)$, where Rc is the value of the crude FRET ratio and Ro is the mean of the baseline. The quantitative results obtained for each neuronal compartment were grouped together and the mean FRET ratio normalized to baseline and SEM were calculated for each time point. Deviation was corrected for somata and dendrites on MATLAB. The mean slope was calculated for all neurons in the somata and dendrites, respectively, for the last 7 time points before addition of treatment and subtracted from all FRET ratio time points.

Imaging of SponGee targeting

Confocal images were acquired with a 63x oil immersion objective (N.A. 1.45) and a Z stack containing the whole specimen was sampled at Nyquist frequency in an Olympus confocal microscope (FV1000). Images were rendered in ImageJ and Photoshop.

QUANTIFICATION AND STATISTICAL ANALYSIS

No data were excluded from the analysis. No sample size calculation was performed. Sample size was considered sufficient after three reproducible and independent experiments, leading to $n \geq 3$ since several animals, coverslips, or biochemical assays were often analyzed for the same experimental condition. Animals or cultures were equivalent and not distinguishable one from another before treatment, de facto randomizing the sample without the need of a formal randomization process. Photomicrographs were often easily traceable by eye to its experimental condition, making blind analysis of the data difficult to achieve. When careful blinding was performed, experiments reproduced the results obtained in non-blinded experiments with identical experimental conditions. Image calculation and analysis were performed using ImageJ, except for the validation of the ^{T}hPDE5^{VV} sensor in hippocampal neurons for which MATLAB was used.

Statistical tests were calculated using GraphPad Prism (GraphPad Software Inc.). Table S1 summarizes the p values and number of replicates.

Cell Reports, Volume *27*

Supplemental Information

SponGee: A Genetic Tool for Subcellular and Cell-Specific cGMP Manipulation

Oriol Ros, Yvrick Zagar, Solène Ribes, Sarah Baudet, Karine Loulier, Sandrine Couvet, Delphine Ladarre, Alain Aghaie, Alice Louail, Christine Petit, Yves Mechulam, Zsolt Lenkei, and Xavier Nicol

SUPPLEMENTAL FIGURES

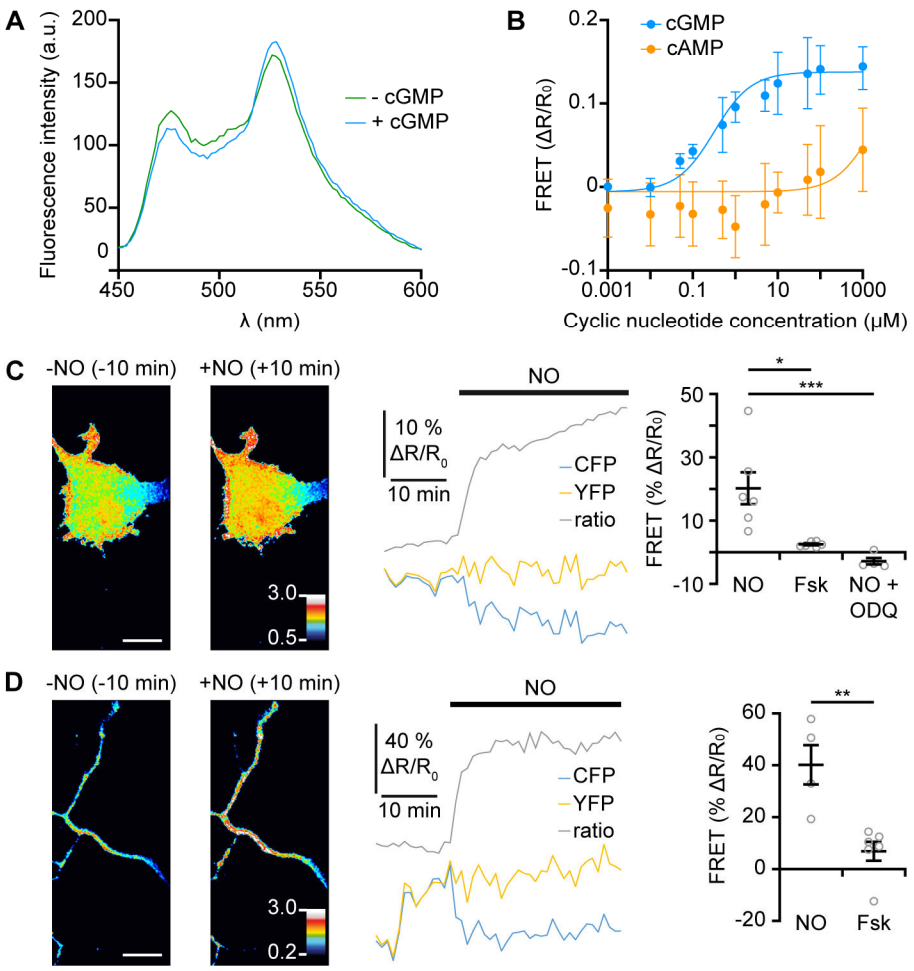

Figure S1. Validation of the ^{T}hPDE5^{VV} biosensor. Related to Figure 2. (A) The emission spectrum of ^{T}hPDE5^{VV} measured from lysates of HEK cells overexpressing the sensor in the absence or presence of cGMP (200 µM). **(B)** Concentration-response curves of ^{T}hPDE5^{VV}. EC50 values are 0.32 ± 0.09 µM for cGMP and 1.6 ± 0.7 mM for cAMP (mean ± S.E.M.). Rat hippocampal cultured neurons were transfected with ^{T}hPDE5^{VV} and imaged using FRET videomicroscopy. Addition of DEA-NONOate 50 µM induced a strong increase of the FRET ratio both in **(C)** the soma and **(D)** axon compared to their respective baselines. In contrast, the adenylyl cyclase activator Forskolin (Fsk, 50 µM) did not induce any FRET elevation. Preincubation of the guanylyl cyclase inhibitor ODQ (100 µM, 10 min before 50 µM DEA-NONOate) blocked the elevation of FRET induced by the NO donor. Representative traces are shown. Data are mean ± s.e.m with individual data points, ** $P < 0.01$, *** $P < 0.001$. **(A)** Kruskal-Wallis test and individual Mann-Whitney tests. **(B)** Mann-Whitney test. Scale bars, 10 µm. Exact *P* values and number of replicates are provided in Table S1.

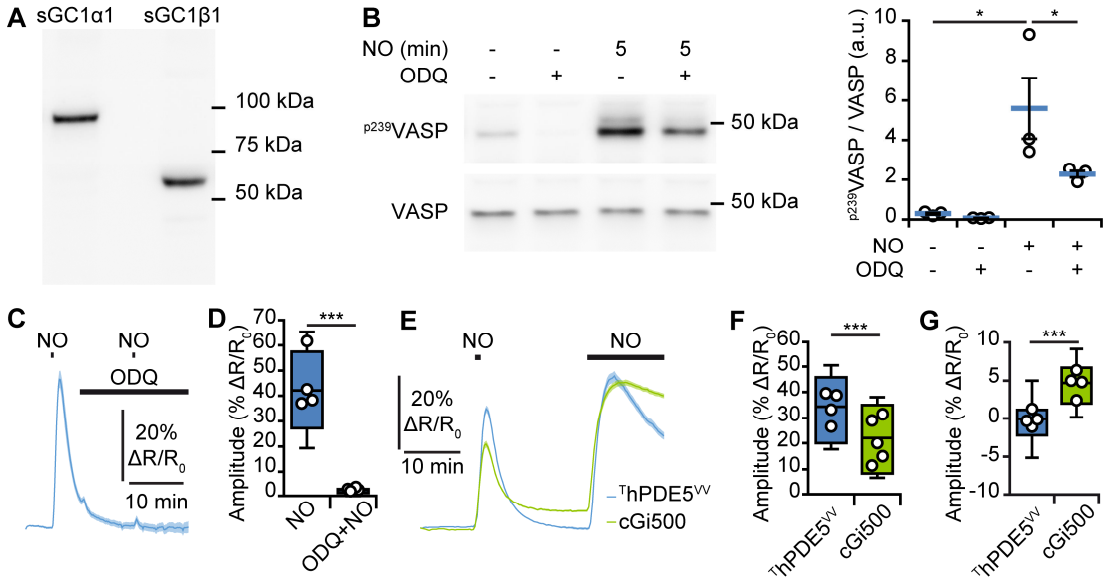

Figure S2. NO-exposed HEK293 cells activate cGMP-dependent signaling and induce sGC-dependent FRET change detected using two distinct FRET sensors. Related to Figure 2. (A) Antibodies directed against the α1 and β1 subunits of soluble guanylyl cyclase 1 (sGC1) detected both subunits in HEK293 cellular extracts. **(B)** In HEK293 cells, NO (Spermine-NONOate 50µM) induced an elevation of the phosphorylated form of VASP at Serine 239, a downstream effector of cGMP. This elevation is reduced by the soluble guanylyl cyclase inhibitor ODQ (100 µM). **(C,D)** A 1-minute pulse of 50 µM Spermine-NONOate (NO) induces an elevation of the FRET:CFP ratio of ^{T}hPDE5^{VV} that was blocked by the sGC inhibitor ODQ (100 µM). **(E,F)** Likewise, a second cGMP FRET probe, cGi500, detected a NO-dependent increase in the CFP:FRET ratio in HEK293. **(F)** cGi500 response to a short pulse of NO was reduced as compared to ^{T}hPDE5^{VV}. **(E,G)** The reversibility of the ratio FRET change was incomplete when using cGi500, in contrast to ^{T}hPDE5^{VV}. **(G)** Quantification of the FRET change after NO washout. **(B)** Data are mean ± s.e.m with individual data points, * $P < 0.05$, one-way ANOVA and Newman-Keuls post hoc tests. **(C,E)** Data are mean ± s.e.m. **(D,F,G)** Box-and-whisker plot elements: center line, mean; box limits, upper and lower quartiles; whiskers, s.d.*;* Mean values for single coverslips (circles) are shown to check for nesting effects. Mann-Whitney test, *** $P < 0.001$. Exact *P* values and number of replicates are provided in Table S1. Data shown in Figure 2B,C are included here for additional comparisons. CFP and YFP traces together with individual cell examples are provided in Figure S7.

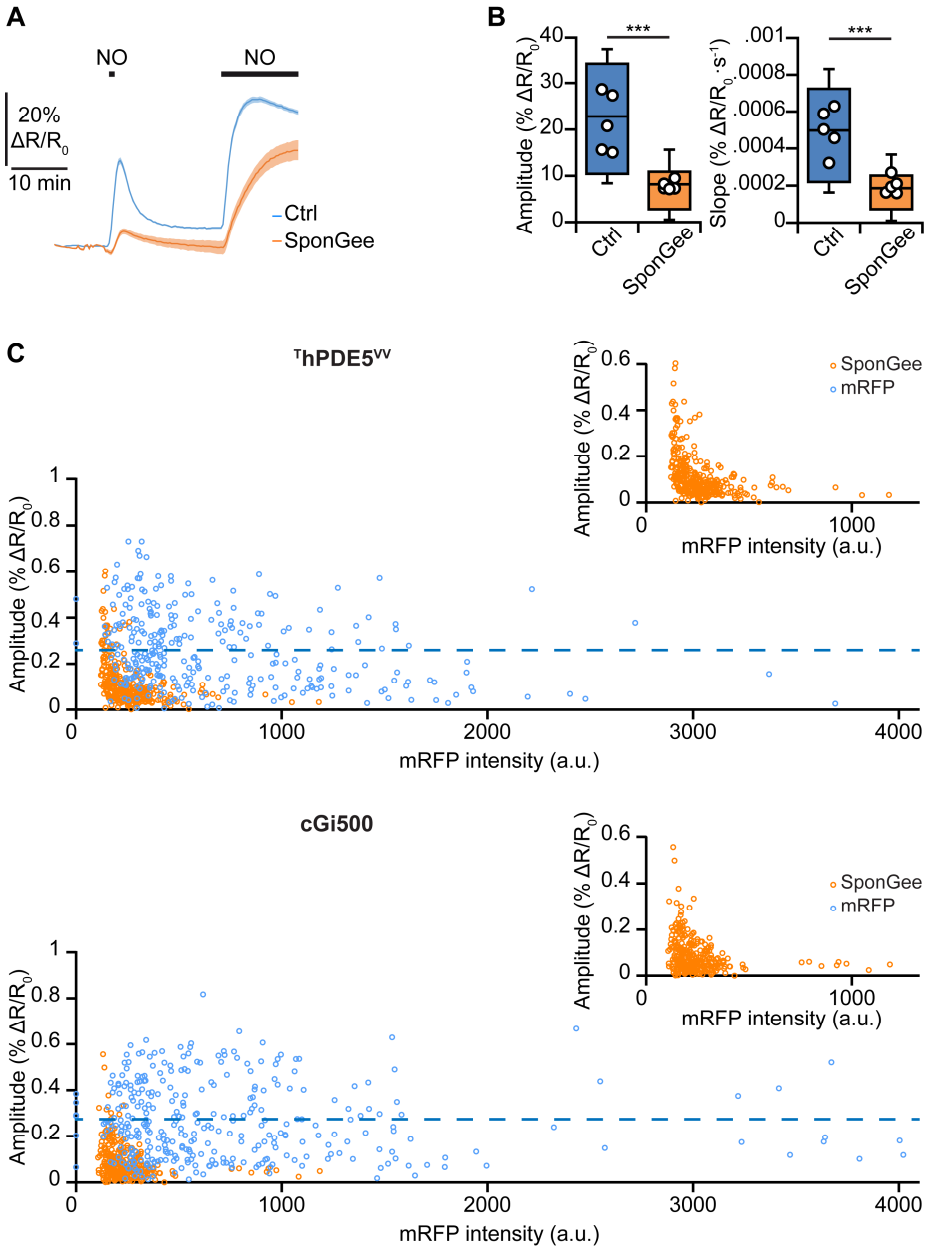

Figure S3. Buffering of NO-induced cGMP elevation by SponGee is detected by cGi500 and is efficient from low levels of expression. Related to Figure 2. **(A)** Cells co-expressing cGi500 and either mRFP or SponGee were challenged with a 1-minute pulse of Spermine-NONOate (50 µM), followed by a sustained exposure. **(B)** SponGee-expressing cells exhibited a reduced response amplitude and rate of elevation of intracellular cGMP concentration. **(C)** The amplitude of cGMP elevation (change in the FRET:CFP or CFP:FRET ratio for ^{T}hPDE5^{VV} and cGi500 respectively) induced by a 1-minute pulse of Spermine-NONOate (50 µM) is plotted against the red fluorescence intensity of mRFP- or SponGee-expressing cells. In the vast majority of SponGee-expressing cells, the amplitude of the elevation in the ratio is smaller than the mean response of the mRFP-expressing cells (dashed line). These observations do not rely on the use of a specific FRET sensor and are reproduced for ^{T}hPDE5^{VV} (top) and cGi500 (bottom). **(A)** Data are mean ± s.e.m. **(B)** Box-and-whisker plot elements: center line, mean; box limits, upper and lower quartiles; whiskers, s.d.; Mean values for single coverslips (circles) are shown to check for nesting effects. Mann-Whitney test, *** $P < 0.001$. Exact P values and number of replicates are provided in Table S1. Data shown in Figure S2 are included here for additional comparisons. CFP and YFP traces together with individual cell examples are provided in Figure S7.

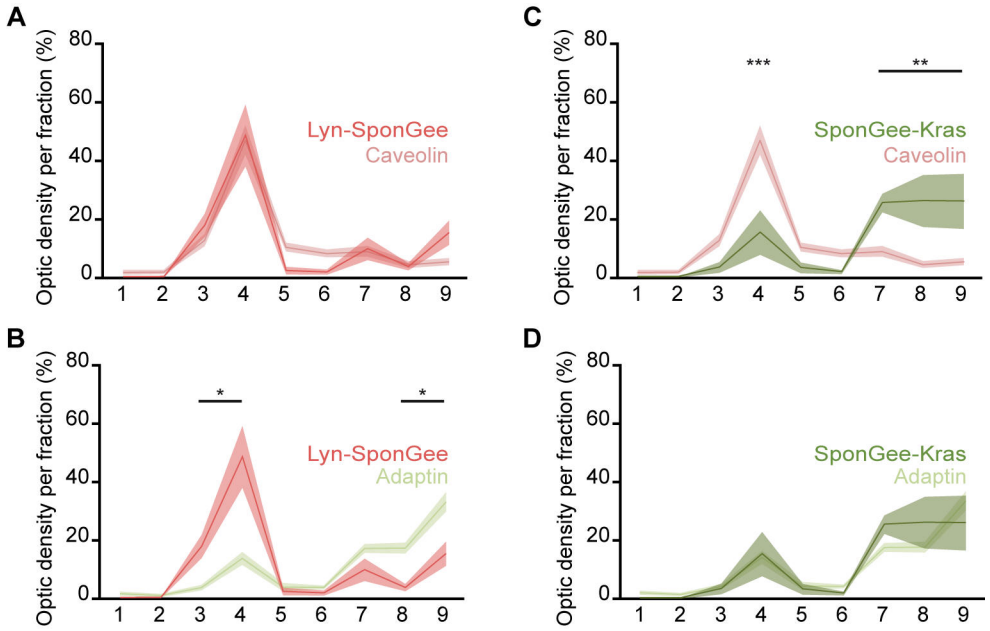

Figure S4. Biochemical characterization of the SponGee targeting. Related to Figure 7. Lyn-SponGee is enriched in fraction 4 on a membrane fractionation assay. **(A)** It coincides with the expression profile of the lipid raft-targeted protein caveolin and **(B)** differs from the submembrane location of adaptin (enriched in fractions 7, 8 and 9), a protein excluded from lipid rafts. SponGee-Kras is enriched in fractions 7-9, with a profile **(C)** distinct from caveolin, and **(D)** similar to adaptin. Data are mean ± s.e.m.; * $P < 0.05$; ** $P < 0.01$; *** $P < 0.001$; Two-way ANOVA and Bonferroni post hoc tests. Exact P values and number of replicates are provided in Table S1. Data shown in Figure 7D are included here for additional comparisons. Individual data points are shown in Figure 7D when $n \leq 10$.

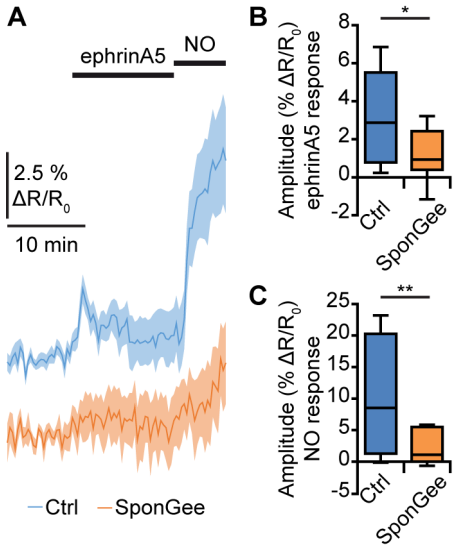

Figure S5. In RGC growth cones, SponGee buffers the ephrinA5-induced increase in cGMP. Related to Figure 7. (A) Control and SponGee-expressing axons were superfused with ephrinA5 (500 ng·mL^{-1}) and Spermine-NONOate (50 µM), and changes in the growth cone cGMP concentration were monitored using ^{T}hPDE5^{VV}. SponGee-expression reduced the increases in cGMP concentration induced by **(B)** ephrinA5 (quantified as the mean amplitude from 0.7 to 2 minutes after ephrinA5 application) and **(C)** NO (quantified as the mean amplitude from 2.7 to 4 min after NO application). **(A)** Data are mean ± s.e.m. **(B,C)** Box-and-whisker plot elements: center line, mean; box limits, upper and lower quartiles; whiskers, s.d. Mann-Whitney test, **P* < 0.05, ***P* < 0.01. Exact *P* values and number of replicates are provided in Table S1. CFP and YFP traces together with individual growth cone examples are provided in Figure S7.

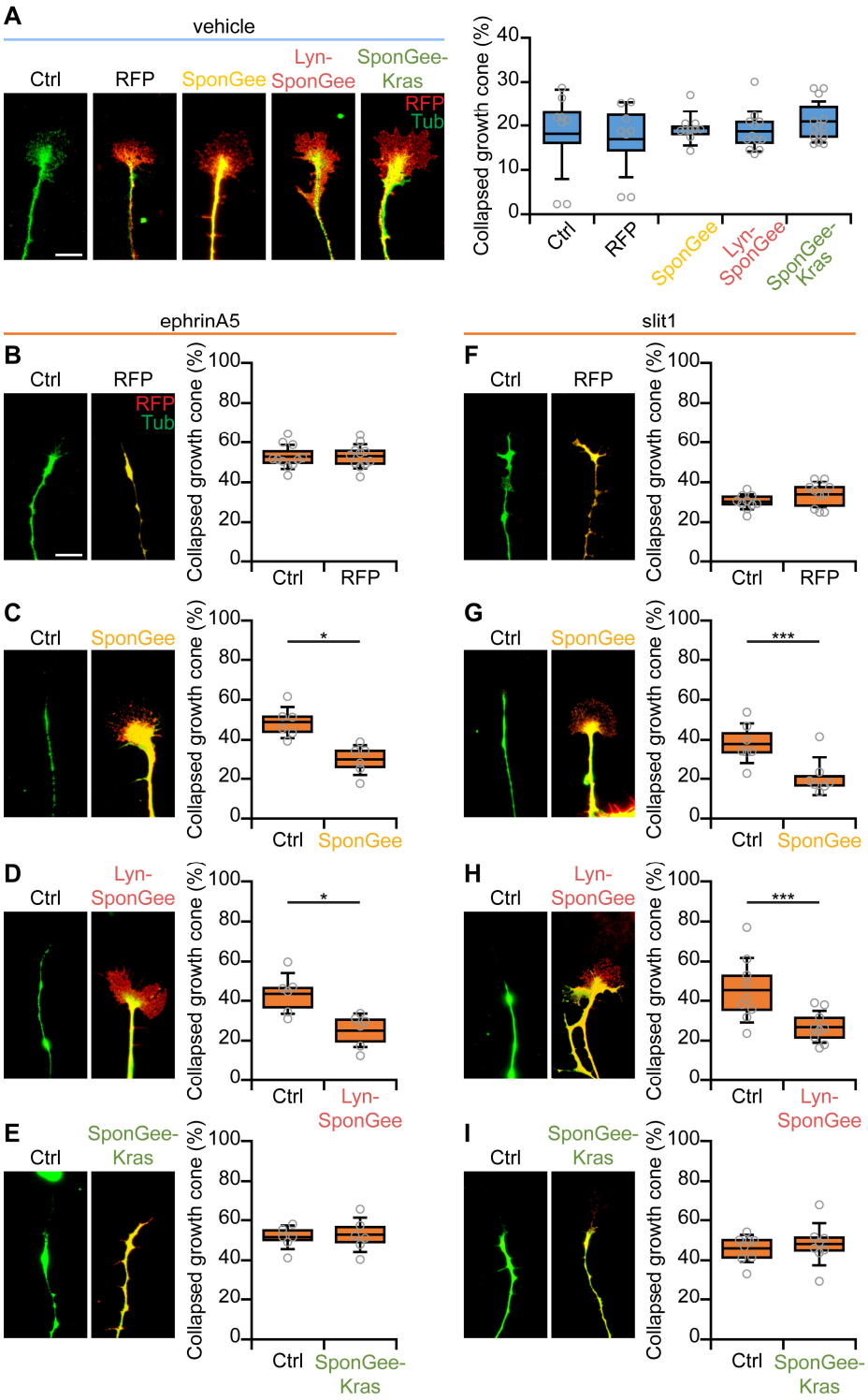

Figure S6. Cytosolic SponGee and Lyn-SponGee but not SponGee-Kras prevent ephrinA5-induced growth cone collapse. Related to Figure 7. (A) SponGee, Lyn-SponGee and SponGee-Kras do not affect the morphology of growing axons. Non-electroporated (Ctrl) RGC axons display a fan-shaped growth cone at their tip which is not affected by the expression of mRFP, SponGee, Lyn-SponGee or SponGee-Kras. When exposed to **(B-E)** 500 ng·mL^{-1} ephrinA5 or **(F-I)** 200 ng·mL^{-1} slit1, mRFP-expressing growth cones exhibit the same collapse response than their non-electroporated neighbors of the same coverslips, **(C, G)** SponGee- and **(D, H)** Lyn-SponGee-expressing axons are resistant to the repellent activity of ephrinA5 and slit1, that is observed in the non-electroporated axons from the same coverslip. **(E, I)** In contrast, SponGee-Kras-expressing axons exhibit similar growth cone remodeling to their controls. Box-and-whisker plot elements: center line, mean; box limits, upper and lower quartiles; whiskers, s.d. Individual data points are shown. Scale bar, 10 µm. **(A)** No significant differences are detected; Kruskall-Wallis test. **(B-I)** * $P < 0.05$; *** $P < 0.001$; Wilcoxon paired test. Exact P values and number of replicates are provided in Table S1. **(A)** A subset of the data shown in Figure 7E,F are included here for additional comparisons. **(B-I)** A subset of the data shown in Figure 7E,F are included here for additional comparisons with control growth cones from the same coverslips.

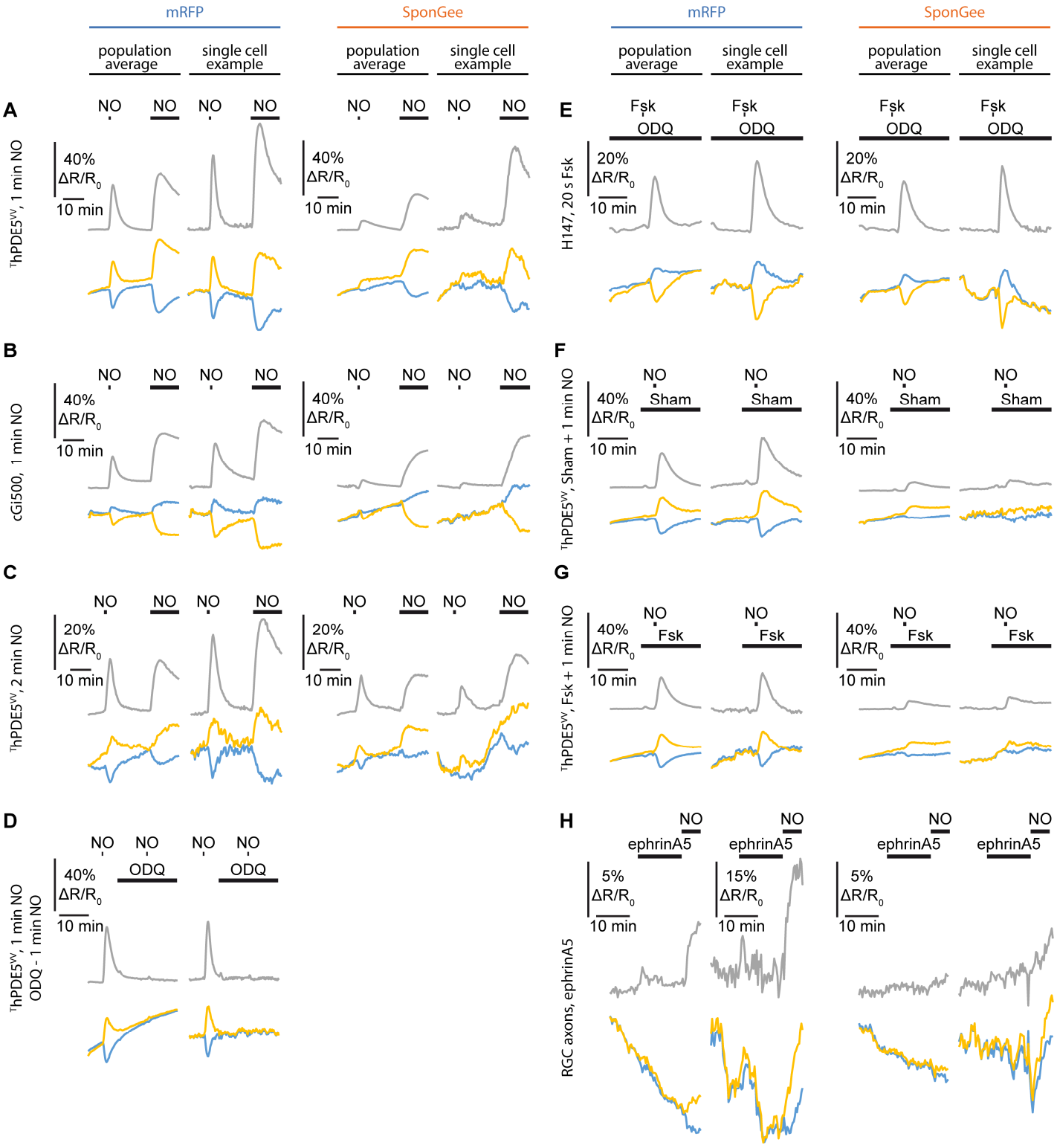

Figure S7. Individual CFP, YFP and Ratio traces. Related to Figure 2, 3, 5, S2, S3 and S5. Average and individual example traces for CFP (blue), YFP (yellow) and ratio are shown for a 1 minute- stimulation of NO using **(A)** ^{T}hPDE5^{VV} (with and without SponGee) or **(B)** cGi500 (with and without SponGee), **(C)** 2 minute-stimulation of NO (using the ^{T}hPDE5^{VV} biosensor, with and without SponGee) **(D)** 1 minute- stimulation of NO alone and in combination with ODQ (using the ^{T}hPDE5^{VV} biosensor), **(E)** a 20 second-stimulation of Fsk using H147 (with and without SponGee), **(F)** a 1 minute- stimulation of NO in combination with a sham exposure (using the ^{T}hPDE5^{VV} biosensor, with and without SponGee), **(G)** a 1 minute- stimulation of NO in combination with a sustained Fsk exposure (using the ^{T}hPDE5^{VV} biosensor, with and without SponGee) and **(H)** an ephrin-A5 stimulation followed by a NO exposure (using the ^{T}hPDE5^{VV} biosensor, with and without SponGee). **(A-G)** HEK293 cells; **(H)** retinal ganglion cells growth cones.